2021

Oil fate and mass balance for the Deepwater Horizon oil spill

Deborah P. French-McCay

Katherine Jayko

Zhengkai Li

Malcolm Spaulding
University of Rhode Island, spaulding@uri.edu

Deborah Crowley
University of Rhode Island

See next page for additional authors

Citation/Publisher Attribution

French-McCay, D. P., Jayko, K., Li, Z., Spaulding, M. L., Crowley, D., Mendelsohn, D.,...Rowe, J. J. (2021). Oil fate and mass balance for the Deepwater Horizon oil spill. *Marine Pollution Bulletin, 171*, 112681. https://doi.org/10.1016/j.marpolbul.2021.112681
Available at: https://doi.org/10.1016/j.marpolbul.2021.112681

Marine Pollution Bulletin 171 (2021) 112681

Contents lists available at ScienceDirect

Marine Pollution Bulletin

journal homepage: www.elsevier.com/locate/marpolbul

Oil fate and mass balance for the Deepwater Horizon oil spill

Deborah P. French-McCay [a,*], Katherine Jayko [a], Zhengkai Li [b], Malcolm L. Spaulding [c], Deborah Crowley [d], Daniel Mendelsohn [a], Matthew Horn [a], Tatsusaburo Isaji [a], Yong Hoon Kim [e], Jeremy Fontenault [a], Jill J. Rowe [a]

[a] RPS Ocean Science, South Kingstown, RI, USA
[b] Center for Drinking Water Quality, Rhode Island Department of Health, Providence, RI, USA
[c] Department of Ocean Engineering, University of Rhode Island, Narragansett, RI, USA
[d] Graduate School of Oceanography, University of Rhode Island, Narragansett, RI, USA
[e] Department of Earth and Space Sciences, West Chester University of Pennsylvania, West Chester, PA, USA

ARTICLE INFO

Keywords:
Oil fate model
Oil mass balance
Oil budget
Oil and gas blowout
Dispersant effectiveness
Oil droplet size distribution

ABSTRACT

Based on oil fate modeling of the Deepwater Horizon spill through August 2010, during June and July 2010, ~89% of the oil surfaced, ~5% entered (by dissolving or as microdroplets) the deep plume (>900 m), and ~6% dissolved and biodegraded between 900 m and 40 m. Subsea dispersant application reduced surfacing oil by ~7% and evaporation of volatiles by ~26%. By July 2011, of the total oil, ~41% evaporated, ~15% was ashore and in nearshore (<10 m) sediments, ~3% was removed by responders, ~38.4% was in the water column (partially degraded; 29% shallower and 9.4% deeper than 40 m), and ~2.6% sedimented in waters >10 m (including 1.5% after August 2010). Volatile and soluble fractions that did not evaporate biodegraded by the end of August 2010, leaving residual oil to disperse and potentially settle. Model estimates were validated by comparison to field observations of floating oil and atmospheric emissions.

1. Introduction

Most modeling studies of the 2010 Deepwater Horizon (DWH) oil spill evaluated the oil trajectory or sensitivity to assumed oil droplet sizes released to the environment (Mariano et al., 2011; MacFadyen et al., 2011; North et al., 2011, 2015; Liu et al., 2011; Le Hénaff et al., 2012; Dietrich et al., 2012; Paris et al., 2012; Lindo-Atichati et al., 2016; Aman et al., 2015; Boufadel et al., 2014; Weisberg et al., 2017; Testa et al., 2016; Hole et al., 2019). A few studied gas and oil fate processes in the buoyant plume, its intrusion into deep water, the inferred rise to the surface, and atmospheric emissions on specific dates (i.e., for 8–10 June 2010; Ryerson et al., 2011, 2012; Gros et al., 2016, 2017; Cooper et al., 2021). The present modeling analysis uniquely quantifies and verifies the full oil fate and mass balance for the DWH spill over the period from the start of spill until the end of August 2010. As gas components (C1–C4 alkanes) dissolved at depth (Valentine et al., 2010; Kujawinski et al., 2011; Kessler et al., 2011; Ryerson et al., 2011, 2012; Reddy et al., 2012; Gros et al., 2017) and would not contribute much to water column toxicity (Paquin et al., 2018), only oil (C5+) fate was modeled as a complete mass balance.

Our results challenge some assertions regarding the fraction of oil that remained at depth versus rising to surface waters, and the degree to which dispersants affected the fate of the oil. Results of extensive trajectory analyses for the spill are available in French-McCay et al. (2018a, 2018c, 2021a). The present paper describes the model inputs, assumptions and results, quantifying mass balance. The results were validated by comparisons to field data related to floating oil and atmospheric emissions (discussed herein) and to detailed analyses of chemical compositional measurements of samples from >900 m depth, presented in a companion paper (French-McCay et al., 2021b).

2. Methods

2.1. Oil spill models

Oil mass balance was evaluated using nearfield buoyant plume and

* Corresponding author.
E-mail addresses: Debbie.FrenchMcCay@rpsgroup.com (D.P. French-McCay), zhengkai.li@health.ri.gov (Z. Li), spaulding@uri.edu (M.L. Spaulding), dcrowley@uri.edu (D. Crowley), daniel.mendelsohn@gmail.com (D. Mendelsohn), matt.horn@rpsgroup.com (M. Horn), YKIM@wcupa.edu (Y.H. Kim), Jeremy.Fontenault@rpsgroup.com (J. Fontenault), Jill.Rowe@rpsgroup.com (J.J. Rowe).

https://doi.org/10.1016/j.marpolbul.2021.112681
Received 3 April 2021; Received in revised form 24 June 2021; Accepted 25 June 2021
Available online 8 July 2021

farfield Lagrangian transport and fate models (Fig. 1). In the nearfield, the oil and gas release started as a momentum-dominated jet, which after a short distance (<1 m; Camilli et al., 2010; Spaulding et al., 2015, 2017) developed into a turbulent buoyant plume. Integral plume models (Rye, 1994; Rye and Brandvik, 1997; Spaulding et al., 2000; Johansen, 2000, 2003; Yapa et al., 2001; Chen and Yapa, 2002; Zheng et al., 2003; Socolofsky and Adams, 2002; Socolofsky et al., 2011, 2015a, 2015b; Johansen et al., 2013; Gros et al., 2017; Spaulding et al., 2017) address the buoyant plume phase of such a release until it has entrained sufficient seawater to reach a neutrally buoyant "trap height", forming an intrusion in the water column, or until the plume has breached the water surface. RPS's (RPS Group Plc) integrated plume model OILMAP DEEP (OIL Model Application Package for DEEP water releases; Spaulding et al., 2000; Crowley et al., 2014; Spaulding et al., 2015, 2017) was used herein to predict the characteristics of the buoyant plume, including the trap height at the center of the intrusion layer.

In oil and gas blowouts such as DWH, the initial breakup into gas bubbles and liquid droplets occurs in the buoyant plume and is simulated by gas and droplet size distribution (DSD) models (e.g., Chen and Yapa, 2007; Bandara and Yapa, 2011; Johansen et al., 2013; Zhao et al., 2014a, 2014b, 2015, 2017a; Nissanka and Yapa, 2016; Li et al., 2017a; Spaulding et al., 2017; Boufadel et al., 2020; Cooper et al., 2021). The gas bubble size distribution influences the rise rate of the buoyant plume, which decreases due to gas dissolution and escapement of gas bubbles from the plume. The DSD was estimated using the Li et al. (2017a, 2017b) model, as described by Spaulding et al. (2015, 2017), accounting for the reduction of oil droplet sizes with application of dispersants (Chan et al., 2015). Oil droplets were released from the intrusion into the farfield environment where their further movements were governed by ambient currents, turbulence, and their individual buoyancy. The physical/chemical changes (i.e., weathering) of the oil droplets, and their movements (with buoyancy affected by weathering), were tracked by the farfield model. Recent analyses by Boufadel et al. (2020) support this approach, where particle transport above the initial intrusion of a multiphase plume in stratified water column is modeled as passive Lagrangian transport.

The 3-dimensional oil spill transport and fate model SIMAP (Spill Impact Model Application Package; French-McCay, 2003, 2004; French-McCay et al., 2004, 2015a, 2018b) was used to evaluate the farfield fate and mass balance of the DWH oil (C5+). As oil is a mixture of thousands of compounds, they were grouped by similar physical-chemical properties into "pseudo-components", where each behaved as if a single chemical with characteristics typical of the group (Payne et al., 1984; Kirstein et al., 1987). As in recent model applications (French-McCay et al., 2015a, 2016, 2018a, 2018b, 2018c, 2018d, 2019), compounds were binned into 18 pseudo-components: nine volatile soluble and semi-soluble (S&SS), eight volatile insoluble, and residual oil (defined in Table A-1, Appendix A, Supporting Information [SI]). The S&SS pseudo-components included monoaromatic hydrocarbons (MAHs, such as benzene, toluene, ethylbenzene and xylene; BTEX), polycyclic aromatic compounds (PACs, which include polycyclic aromatic hydrocarbons, PAHs, and related heterocyclic compounds that contain S, N, or O), and soluble alkanes. The model tracked these pseudo-components in droplet and dissolved phases of the water column, sediments, floating oil, and shorelines. Weathering and transport processes modeled included spreading (gravitational and by shearing), evaporation of 17 volatile pseudo-components from surface oil, transport on the surface and in the water column from ocean currents, dispersion from small-scale motions (mixing), emulsification, entrainment of oil as droplets into the water (natural and facilitated by surface dispersant application), dissolution of the 9 S&SS pseudo-components, volatilization of dissolved compounds from the surface wave-mixed layer, adherence of oil droplets to suspended particulate matter (SPM), adsorption of S&SS compounds to SPM, sedimentation, stranding on shorelines, and degradation (pseudo-component-specific biodegradation and photo-oxidation). Appendix A (SI) contains a summary of the model algorithms and assumptions; detailed descriptions are provided in French-McCay et al. (2018b, 2018c).

2.2. Prior modeling studies of DWH oil spill by the authors

OILMAP DEEP (Spaulding et al., 2015, 2017; Appendix B [SI]) and

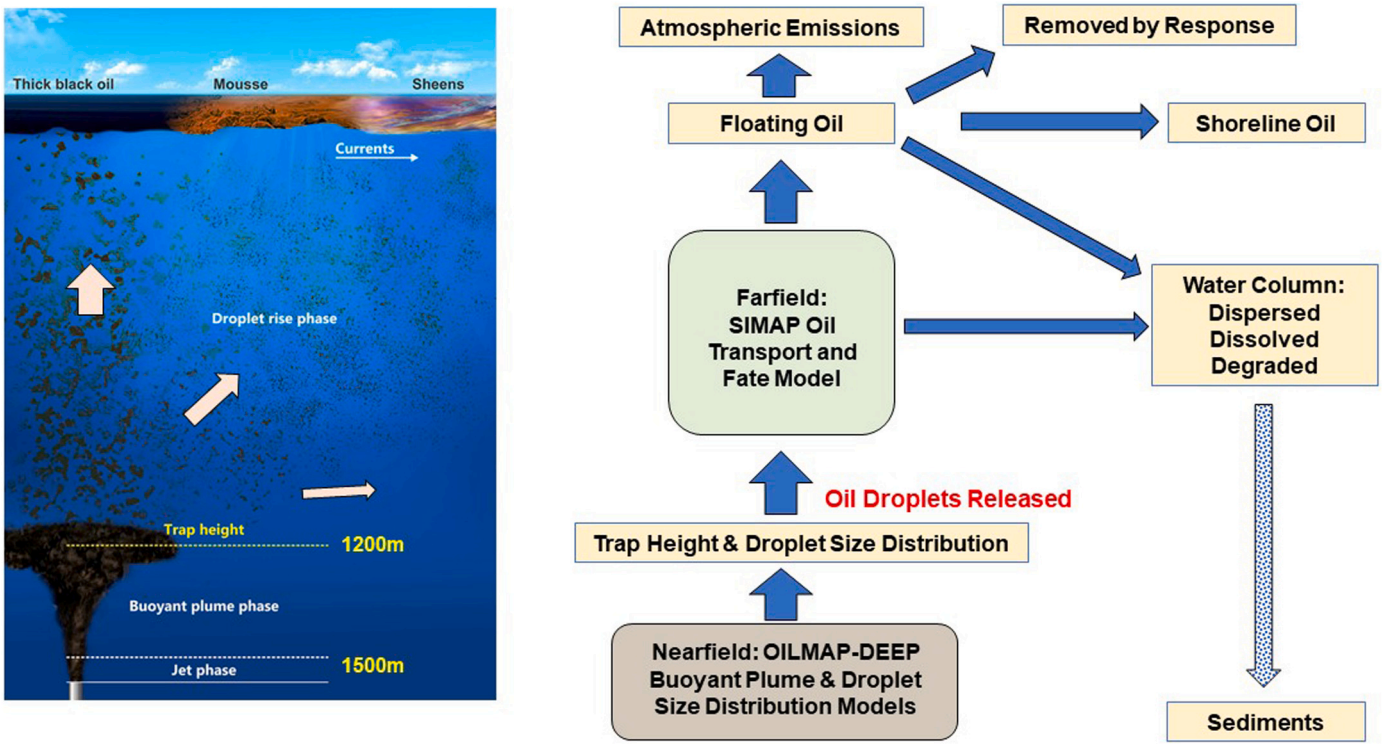

Fig. 1. Conceptual model of the buoyant plume, rising oil droplets, and far field transport and fate.

SIMAP (French-McCay et al., 2015a, 2015b, 2015c, 2015d, 2015e, 2016) were used to evaluate the DWH oil spill in support of the Natural Resource Damage Assessment (NRDA) by the DWH Trustees (2016). Simplifying assumptions regarding transport were used to estimate exposures to aquatic biota below 20 m (depth of surface mixed layer) and within a 25 km by 25 km box surrounding the wellhead (French-McCay et al., 2015a, 2016). French-McCay et al. (2015a, 2016, 2018a, 2018c) showed that model-predicted concentrations of S&SS components below 20 m and within 10–15 km of the wellhead agreed in magnitude with measured concentrations from field samples.

French-McCay et al. (2018a, 2018c, 2021a) describe additional analyses and modeling of the DWH spill through examination of transport and oil distributions. Those results were compared to remote sensing-based observations of floating oil, shoreline oiling distributions from surveys, fluorescence and other sensor data indicating the path of the deep plume/intrusion layer, and chemistry sample data. Several model inputs were varied to quantify uncertainty and determine which provided the best fit to observations, including currents from seven different hydrodynamic models and measurements by Acoustic Doppler Current Profilers (ADCPs), winds from four meteorological models, horizontal turbulent dispersion coefficients, and surface oil wind drift. The mass balance calculated with SIMAP was not sensitive to the wind and current data set used as input (except for the amount coming ashore versus entrained in the water column, due to differential transport in nearshore areas), or to the assumed dispersion coefficients or wind drift assumptions. The direction and speed of transport in the offshore environment did not greatly affect the fate processes and so did not significantly affect the mass balance. Thus, comparison of the model and observed trajectories are not reviewed here, but are provided in French-McCay et al. (2015a, 2018a, 2018c, 2021a). Based on these model simulations, one set of forcing data, that which led to the best fit with the observations overall (described in Section 2.6), was used for the model simulations examined herein.

2.3. Release locations and volumes

The spill location (Fig. C-2, Appendix C, SI) was ~80 km southeast of the mouth of the Mississippi River in ~1500 m of water (in Mississippi Canyon Block 252, MC252). The daily release rates of oil to the environment (totaling 4.127 million bbl; ~656,000 m^3; ~554,000 metric tons, MT; i.e., not including the amount recovered at the release site; Lehr et al., 2010; McNutt et al., 2012a) and associated daily-specific DSDs were input to SIMAP from 22 April 2010 for 84 days (until 15 July 2010; Sections B.2, B.3.1, Appendix B, SI). From April 28 to June 3, oil and gas flowed from both the broken end of the fallen riser and holes in a kink in the riser pipe just above the blowout preventor (BOP). After June 3, oil was released only from the riser pipe and around the top hat immediately above the BOP. The droplet diameters from the riser flows (~2–3 mm) were significantly larger than those from the kink hole flows (~300–500 μm), due to the much higher exit velocity from the kink holes relative to the larger diameter riser.

2.4. Nearfield modeling

As described in Spaulding et al. (2015, 2017; summarized in Section B.3, Appendix B, SI), OILMAP DEEP was used to estimate the trap height (s) on each day of the release. The DSDs were estimated for each day of release based on oil and gas flow rates from each source (kink holes and end of the riser), the turbulent energy in the discharge plumes, and oil properties, considering the daily-varying dispersant volumes used for subsea dispersant injection (SSDI; Spaulding et al., 2015, 2017; Li et al., 2017a). Dispersants were applied at the outer edge of the discharge plume from the end of the riser via a single wand or multipronged trident. The analysis explicitly considered the presence of the top hat placed on June 3 over the cut riser to collect oil from the well. The oil mass, DSD, and trap depth for each day were used as input to SIMAP to simulate the oil fate in the farfield.

Spaulding et al. (2015, 2017) evaluated three dispersant-treatment case assumptions. One was considered the most realistic, while the others bounded the range of DSDs that could have been released at the trap height, based on the uncertainties of the model assumptions:

- Bimodal Partial-Treatment Base Case (most realistic): Before the riser was cut on June 3, dispersants were applied by a single wand to part (estimated as 8.1%) of the plume flow from the end of the fallen riser. After June 3, ~30% of the oil and gas plume was treated (much of the time using a multipronged trident) as it escaped recovery at the outer edge of the top hat. The dispersant (contact) effectiveness with the liquid oil in the treated fraction was estimated as 80% (i.e., yielding 6.5% effectively treated before June 3, and 24% after). The partial treatment of the riser release led to a bimodal distribution of droplet sizes, with a peak of smaller droplets representing the treated fraction and the peak of larger droplets representing untreated oil.
- High Dispersant Effectiveness Case: Dispersants were assumed to completely mix in the plume flow with 100% effectiveness (application to the liquid oil phase), i.e., the maximum possible effectiveness, bounding the problem.
- Low Dispersant Effectiveness Case: Dispersants were assumed to completely mix in the plume flow with 50% effectiveness (i.e., low end estimate with only 50% of the dispersant assumed to treat the liquid oil in the buoyant plume).

The modeled DSD varied daily, based on release conditions, flow rate and dispersant quantity applied each day. Prior to June 3, the releases through the kink holes (which were not treated with dispersant) generated small droplet sizes (<1 mm) due to high exit velocities and resulting turbulence. The assumptions for the bimodal partial-treatment model for the riser flows were derived from an in-depth analysis of remotely operated vehicle (ROV) videos of the release and SSDI treatments (see Appendices of Spaulding et al., 2015 and Section B.3, Appendix B, SI). In May, a single-wand applicator was held next to the buoyant plume from the riser and the dispersant entrained into the side of the plume. Post riser cut, after June 3, Top Hat #4 placed over the cut riser had an attached pipe leading to the surface, through which some of the oil and gas mixture was recovered. In addition to rising through the pipe, the oil and gas plume flowed through the annulus-shaped gap between the top hat and the cut riser, flowing around the top hat and upwards surrounding the recovery pipe. Thus, after June 3, the buoyant plume surrounded the pipe and was not a simple continuous plume. Rather, limited mixing occurred around the circumference of the plume that encompassed the pipe. This is one of the factors Spaulding et al. (2015, 2017) considered, along with the video of the release and dispersant treatment techniques, that indicated partial treatment of the plume by the dispersant application, such that treated oil was in smaller droplet sizes than the untreated oil, which together formed a bimodal DSD. (See Spaulding et al., 2015, 2017 for details). The assumptions used to apply the Li et al. (2017a) DSD model to the three above cases are in Section B.3.2, Appendix B (SI).

Calculations of daily-varying trap heights, dispersant-to-oil ratios, and resulting DSDs by source (kink holes or riser) are unique to this modeling effort. No other modeling study has considered these important sources of variation. Other published models have assumed a single source point, complete mixing of the dispersant into the plume, and constant oil and gas release rates either for the entire spill (e.g., Paris et al., 2012; Perlin et al., 2020) or focusing on the early June 2010 conditions (Zhao et al., 2015; Gros et al., 2017; Boufadel et al., 2018; Cooper et al., 2021). (See further discussion in Section B.3.4, Appendix B, SI).

2.5. Oil properties and composition

The bulk properties of the oil released to the farfield were measured

by Stout (2015b) using oil collected on 21 May 2010 from the riser insertion tube that was receiving oil and gas directly from the well's broken riser near the sea floor. Concentrations of S&SS compounds (from Stout, 2015a; Stout et al., 2016a) were very similar to those measured by Reddy et al. (2012) for a sample taken just above the wellhead on 21 June 2010. It was assumed that aqueous dissolution of the C5+ compounds within the buoyant plume was negligible, since the rise time to the trap height was ~15–20 min. For the SIMAP simulations, each of the modeled pseudo-components (C5+) were assigned initial concentrations in the oil phase and physical-chemical properties (Section B.1, Appendix B, SI), as well as empirically based photo- and biodegradation rates (Section C.1.8, Appendix C, SI), which were mass-weighted means of rates for the individual compounds.

2.6. Environmental data inputs

Spatially varying data defining bathymetry, shore/habitat types, currents, winds, SPM concentrations, water temperature and salinity, and horizontal and vertical diffusion coefficients are described in Section C.1, Appendix C (SI). Currents from the HYbrid Coordinate Ocean Model (HYCOM) simulation, implemented by Florida State University (FSU; Chassignet and Srinivasan, 2015), yielded the best overall trajectory of the seven hydrodynamic models tested (French-McCay et al., 2018a, 2018c, 2021a). Data from 18 ADCPs at 17 stations (including three within 8 km of the release locations, and all at depths greater than 40 m) were interpolated to develop three-dimensional and time-varying current fields using an inverse distance-weighted scheme. ADCP-based trajectories more closely agreed with subsurface oil observations than the HYCOM-FSU simulation (French-McCay et al., 2018a, 2018c) or any of the other hydrodynamic model results considered. Thus, we present here the mass balance and related results of the SIMAP simulations run with a combination of ADCP currents below 40 m and HYCOM-FSU currents in waters above 40 m. Wind data were obtained from the National Oceanic and Atmospheric Administration (NOAA) National Center for Environmental Prediction (NCEP) North American Regional Reanalysis (NARR) model, the same as used to force the HYCOM-FSU model.

While Marine Oil Snow Sedimentation and Flocculent Accumulation (MOSSFA; Passow et al., 2012; Fu et al., 2014; Ziervogel et al., 2014; Joye et al., 2014; Chanton et al., 2015; Brooks et al., 2015; Passow, 2016; Passow and Ziervogel, 2016; Quigg et al., 2016; Daly et al., 2016; Stout et al., 2016b, 2017; Romero et al., 2015, 2017; Babcock-Adams et al., 2017; Burd et al., 2020) was recognized as an oil pathway, spill-wide quantitative estimates of organic particulate concentrations due to microbial and phytoplankton growth, exudates, and marine oil snow formation were not available, and so oil sedimentation by this process was not included in the simulations. Additionally, sinking residues from surface oil (in situ) burns and oil sedimentation by suspended sediment and other materials discharged as part of top-kill operations (26–28 May 2010; USDC, 2015; Stout and Payne, 2016b, 2017) were not modeled. However, estimates were made of sedimentation via MOSSFA and included in the final mass budget for the spill.

2.7. Surface response

Modeled response activities at the water surface included removal by in situ burning (ISB) and dispersant application onto floating oil from the air and surface vessels. Spatially explicit quantitative measurements of oil volume mechanically removed were not available, but likely accounted for a small percentage of the spilled oil (see Section 3.3.1). Therefore, mechanical cleanup was not included in the simulations. Polygons identifying the locations, timing, and amounts of dispersant-treated surface oil were input to the model to specify response activities. The sources of these data, as well as model assumptions about the efficacy, acceptable weather conditions, and other response constraints, are provided in Section C.1.10, Appendix C (SI).

2.8. Remote sensing data

Satellite imagery on 84 dates was judged sufficiently synoptic of the area of the floating oil, including 34 Synthetic Aperture Radar (SAR), 18 Moderate Resolution Imaging Spectroradiometer (MODIS) Visible (MVIS), 25 MODIS Thermal IR (infrared) sensor (MTIR) and 7 Landsat Thematic Mapper (TM) images, available from ERMA (2016). Remote sensing (overflight and satellite imagery) data were used to: (1) indicate where oil surfaced (useful for evaluating the modeled DSD), (2) evaluate the distribution of surface oil, and (3) compare volume of floating oil (using estimates of average oil thickness) with model predictions. Methods are described in Section C.2, Appendix C (SI).

3. Results and discussion

3.1. Nearfield modeling

3.1.1. Trap height

Based on the nearfield model analyses (performed for each day of release), the kink releases trapped at 1280–1310 m, whereas the (larger flow rate) releases from the riser trapped at 1150–1220 m (Spaulding et al., 2015; Section B.3.1.1, Appendix B, SI). The rise times to the trap heights were ~15–20 min. Fluorescence and dissolved oxygen anomalies, and chemical concentration measurements, during 2010 (Camilli et al., 2010; Diercks et al., 2010; Valentine et al., 2010; Reddy et al., 2012; Spier et al., 2013; Horn et al., 2015; French-McCay et al., 2015a; Payne and Driskell, 2015b, 2016, 2017, 2018; Driskell and Payne, 2018a, 2018b), as well as model calculations by Socolofsky et al. (2011), indicate that a considerable portion of the buoyant plume trapped at ~1200 m depth. Observations of secondary peaks were centered at ~1300 m. Thus, the model-predicted trap heights are consistent with the field evidence and other analyses (Spaulding et al., 2015, 2017).

3.1.2. Droplet sizes

Modeled oil fate is sensitive to the DSD of the released oil (Chen and Yapa, 2002, 2007; French-McCay, 2008; North et al., 2015; French-McCay et al., 2015a, 2019; Daae et al., 2018). Based on Spaulding et al.'s (2015, 2017) application of the DSD model (Li et al., 2017a), the volume mean diameter (VMD, of a logarithmic distribution, with standard deviation 0.5 based on experimental data) of untreated oil droplets was 2.7–3.0 mm in April–May and 2.5–2.6 mm in June–July. The subsea dispersant application rates, and the resulting dispersant-to-oil ratios, varied over time, becoming more consistent after the riser was cut on June 3 (Figs. B-8 to B-12, Appendix B, SI). During June, the VMD of the dispersant-treated oil (assuming complete mixing of the dispersant within the plume) was ~400 μm for the high treatment case and ~1130 μm for the low treatment case. The VMD during June for the 24% of the oil treated in the bimodal case was ~160 μm, while untreated oil amounted to 76% of the released oil. The modeled DSDs (which varied daily) and discussion of uncertainties are provided in Section B.3.2 (Figs. B-4 to B-7, Appendix B, SI).

Multiple observations of the locations and timing of surfacing oil during the DWH spill confirm that a substantial portion of the released oil mass was in the form of large droplets, >1 mm in diameter, even while SSDI proceeded. Ryerson et al. (2012), Reddy et al. (2012), Spier et al. (2013), Payne and Driskell (2015b, 2015d, 2018), Svejkovsky and Hess (2012), and Svejkovsky et al. (2016) observed that a significant amount of oil reached the surface within 3–12 h (Section C.3.1, Appendix C, SI). The freshest oil observed to surface was collected 2 km from the wellhead (Stout et al., 2016a). Based on the temporally and vertically averaged current velocities of ~4 cm/s at ADCP station #42916 near the wellhead (French-McCay et al., 2015a), and accounting for weathering and the vertical water density gradient, 1.0 and 0.7 mm droplets surfaced 1.5 to 2.4 km from the wellhead, 11 to 17 h after release. Assuming the vertically averaged current speed (~7 cm/s, Spaulding et al., 2015) as unidirectional, to bound the expected

surfacing distance, a 0.7-mm droplet would surface 4.3 km from the well (Figs. C-7 and C-8, Appendix C, SI). Thus, the large amounts of oil observed to be surfacing within 4 km of the well were derived from >0.7 mm droplets.

Assuming average currents, 300 and 150 μm droplets rose to 900 m depth in 16 and 73 h, at ~2 km and ~10 km from the well, respectively (Fig. C-7, Appendix C). C1–C11 compounds dissolved rapidly from these small droplets (Ryerson et al., 2012; Gros et al., 2017), shrinking to 291 and 137 μm in diameter, respectively, based on model predictions (Fig. C-9, Appendix C). Thus, oil droplets >900 m below the surface and 2–10 km from the well were initially <300 μm, and those >10 km from the well were initially <140 μm. Payne and Driskell (2015a, 2015b, 2015c, 2015d, 2016, 2018) found that there was particulate oil in small droplets (<300 μm) in the deep plume when subsea dispersants were applied, as filtered samples had substantial concentrations of dispersant indicators (glycol ethers) and non-soluble alkanes, plus extensively water-washed losses of lower-alkylated homologues within each PAC group. Visible oil fog and rising oil droplets were documented in ROV imagery taken at mid-depths (Payne and Driskell, 2015b, 2017; Li et al., 2015, 2017a). Holographic image analysis (Davis and Loomis, 2014; Li et al., 2015, 2017a) demonstrated measurable numbers of 70–250 μm droplets at 700–1200 m below the surface 1.2–2.1 km from the wellhead, which were at concentrations in agreement with chemistry sample measurements at the same stations (see Section C.3.1, Appendix C).

Based on the bimodal DSD for the release during June 8–10 (Spaulding et al., 2015, 2017), ~79% of the oil was in droplets with diameters >300 μm, which would have surfaced within 10 km from the well. Gros et al. (2017) using VDROP-J predicted that, during June 2010, 0.1%, 1.3%, and 98.6% of the oil was in <130 μm, 130–300 μm, and >300 μm droplets, respectively. However, in modeling their DSD Gros et al. (2017) did not consider the details of the dispersant treatment approach and its effectiveness (via single wand on June 8) and the fact that the oil was being released at the outer edge of the top hat. Based on their comparisons to deep-plume sample chemistry and model calibration, Gros et al. (2017) concluded that ~1.2% of the C10+ was retained in the deep-water intrusion as microdroplets <130 μm in diameter, modifying their DSD accordingly, such that 97.5% of the (oil) mass was >300 μm. Spaulding et al.'s bimodal model estimate for 8 June 2010 was that ~8% of the oil (C5+) was released as <130 μm microdroplets.

Models assuming a single DSD (e.g., Spaulding et al. (2015, 2017) dispersant effectiveness assumption extremes of 0.4–1.1 mm VMD; Gros et al. (2017) VDROP-J estimate with 1.3 mm VMD (and no added microdroplets); and SINTEF model with 1.8 mm VMD (NASEM, 2020)) did not account for enough mass in microdroplets to be consistent with the composition of PACs in chemistry samples taken >900 m (see also French-McCay et al., 2021b). Model scenarios using DSDs assuming a release of most or all of the oil mass in microdroplets with VMD < 130 μm (Paris et al., 2012; Lindo-Atichati et al., 2016; Aman et al., 2015; Perlin et al., 2020; Bracco et al., 2020)) predicted either no oil or negligible amounts of oil surfacing near the wellhead, which is not in accordance with observations of large amounts of surfacing oil near the wellhead (e.g., Ryerson et al., 2012; Reddy et al., 2012; Spier et al., 2013; Payne and Driskell 2015b, 2018) and large droplet sizes subsea (Payne and Driskell, 2015b; Li et al., 2015), nor is it consistent with the physical-chemical conditions of the release (Adams et al., 2013; Gros et al., 2017, 2020; NASEM, 2020; Cooper et al., 2021; see discussion in Section B.3.4, SI and in French-McCay et al., 2021b). Thus, the Spaulding et al. (2015, 2017) bimodal DSD, assuming partial treatment by SSDI, is most consistent with observations and was assumed for the base case in the farfield modeling.

3.2. Farfield trajectory

The uncertainties in the spatial-temporal distributions of oil, which arise from those in wind and ocean current model data used for forcing, are evident when comparing among published oil spill model trajectories for DWH (Adcroft et al., 2010; MacFadyen et al., 2011; Liu et al., 2011; Mariano et al., 2011; Dietrich et al., 2012; Le Hénaff et al., 2012; Kourafalou and Androulidakis, 2013; Jolliff et al., 2014; Boufadel et al., 2014; Goni et al., 2015; North et al., 2011, 2015; Testa et al., 2016; Özgökmen et al., 2016; Weisberg et al., 2017; French-McCay et al., 2018a, 2018c, 2021a). In comparing our model results (French-McCay et al., 2018a, 2018c, 2021a) to surfacing oil locations, remote sensing-based observations (SAR, MVIS, MTIR, and Landsat TM), shoreline oiling distributions, fluorescence and other sensor data, and chemistry sample measurements, the best overall fit was found using interpolated ADCP data in subsurface waters (>40 m) and HYCOM-FSU currents in surface waters (i.e. the base case). The trajectory results for these and other environmental inputs are provided in French-McCay et al. (2015a, 2018a, 2018c, 2021a).

French-McCay et al. (2021a) summarize the floating, shoreline and sediment oil exposure for the base-case model. The predicted number of days of oil cover was found to be in the same range and in similar areas as estimated by the DWH Trustees (2016) based on remote sensing imagery (Graettinger et al., 2015). The shoreline distribution was along the same coastlines identified as oiled by responders (OSAT-2, 2011) and the DWH Trustees (2016; Nixon et al., 2016). The model predicted oil sedimentation in the offshore area surrounding the well site where MC252 oil was identified in the sediments (Joye et al., 2011; Montagna et al., 2013; Valentine et al., 2014; Stout and Payne, 2016a; Stout et al., 2016b; Romero et al., 2015), as well as in nearshore areas of Louisiana to the panhandle of Florida, where oil was measured in sediment samples (OSAT, 2011).

3.3. Mass balance

3.3.1. Model results

Figs. 2 and 3 show the mass balance of the (C5+) oil (as percentage released to date and as mass) by environmental compartment, for the base case using the Spaulding et al. (2015, 2017) bimodal DSD as input. Figs. C-10 and C-11 show the results (as mass) for the bounding low and high effectiveness DSDs, and Figs. C-12 and C-13 (Appendix C) show how the mass balance would have differed if no subsea dispersant was used, with and without burning and surface dispersant applications included. While the differences in the floating and shoreline oil amounts are subtle, the simulations including effective SSDI resulted in considerably more biodegradation in subsurface waters (facilitated by smaller droplets and therefore faster dissolution rates with SSDI) and less volatilization to the atmosphere, particularly in June–July 2010. The effectiveness of SSDI each day varied, and was limited by ability to mix with the escaping oil and the volumes of dispersants applied, such that the resulting dispersant concentrations in the treated oil were typically <1% (<1:100; Fig. B-3, Appendix B).

Because the discharged oil had a high volatile content, much of the surfaced oil evaporated. Oil in the water column included small droplets dispersed at depth, oil droplets entrained by waves from the surface, and dissolved soluble components. Degradation rates were fastest for oil components within the water column; thus, the degraded fractions that accumulated over the simulations were mainly in the water column. A small percentage of water column oil mass settled (see Section 3.3.3), while most mass remained in the water column and biodegraded over time.

Table 1 summarizes the mass balance on 31 August 2010 for model cases varying dispersant-treatment assumptions. (Appendix C.3.3, SI, contains further detail.) By August 31, <0.1% of the oil remained floating, evaporation was complete, and most of the oil that was to reach shorelines had done so. Oil components moving out of the model domain were in the water column and would have continued to biodegrade (with a portion settling) had the simulations continued past the end of August. Thus, in Table 1, the sum of the percentages in the water column, degraded, and out of the domain represents the mass percentage that ultimately degraded in the water column or settled after August 31.

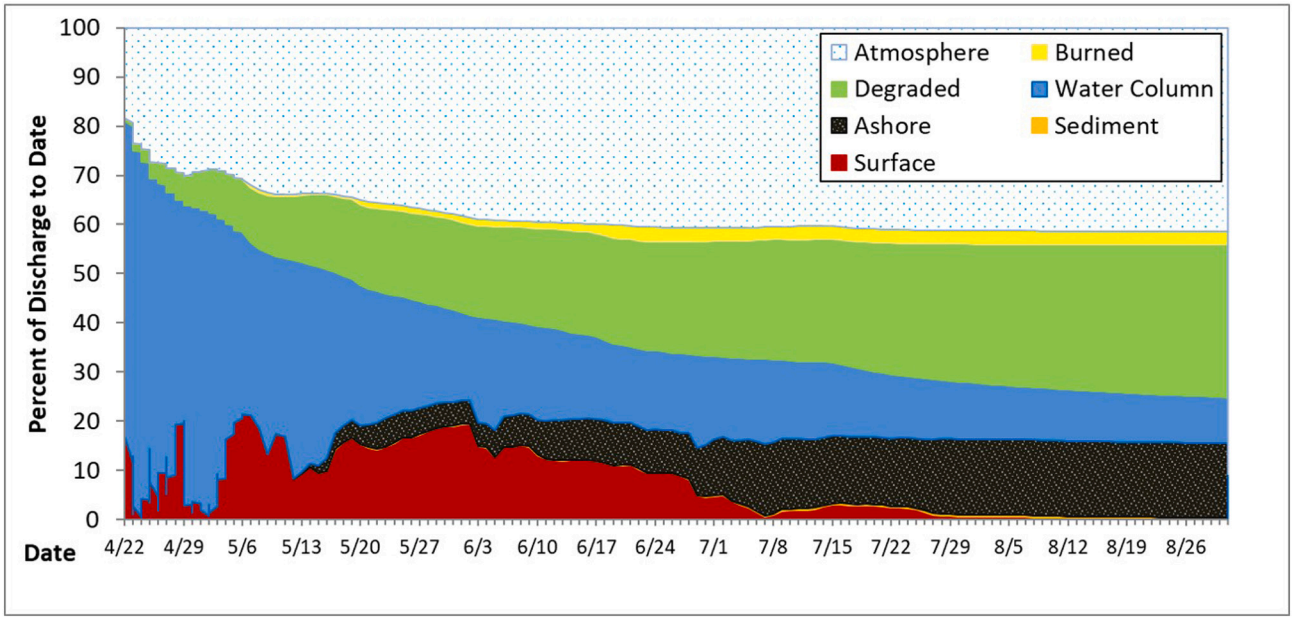

Fig. 2. Mass balance (percentage of discharge to date) in environmental compartments for the base case, assuming the bimodal droplet size distribution.

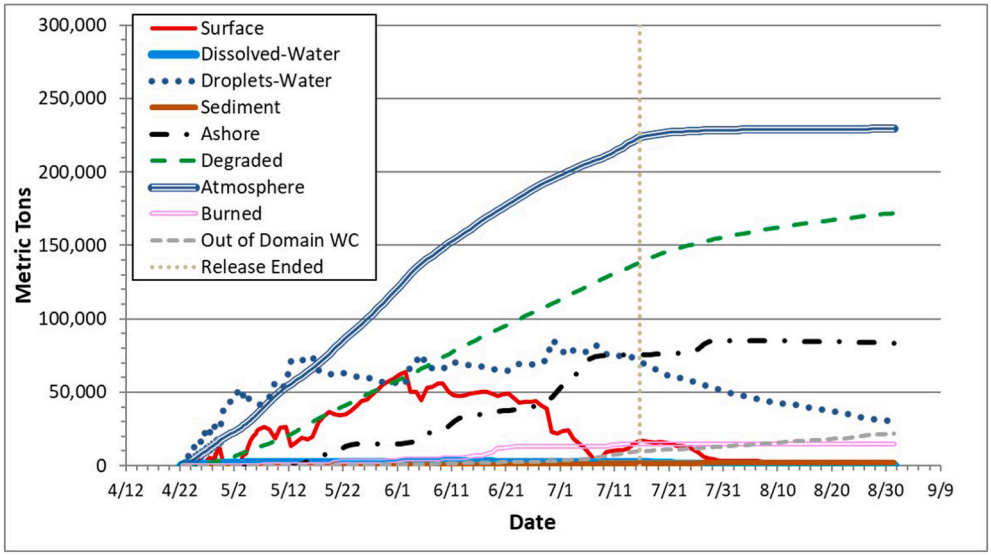

Fig. 3. Mass balance (metric tons) in environmental compartments for the base case assuming the bimodal droplet size distribution.

In Fig. 2, the out-of-domain mass (~4% on August 31, for the base case) was combined with the degraded pool for simplicity. Varying the assumed DSD over the bounding range (i.e., low and high effectiveness SSDI assumptions) affected the mass balance by about ±10% of the base case (Table 1). The simulations run without SSDI (Fig. C-12, Appendix C), resulted in higher floating oil exposure, more oil ashore, more volatilized, and less oil degraded than the base case simulation including SSDI (Table 1).

The best estimates of the oil amounts retained in the water column (without first surfacing) were ~5% below 900 m, ~5% within 900–200 m, and 1% within 200–40 m (40 m being the approximate depth of the surface mixed layer; uncertainty ranges in Table 2). Oil and components retained below 40 m biodegraded in the water column (most of the mass) or settled to the sediments.

An estimated 89.3% of the oil surfaced (Table 2), and of that, 46% evaporated, 17% came ashore, 3% was removed by ISB, and 34% re-entrained into surface waters by natural and dispersant-facilitated dispersion. Of the surfaced oil that did not evaporate, which would be considered "actionable oil" by the responders, 6.3% was burned. By the end of August, of the total spilled oil, ~41% evaporated, ~15% came ashore, ~2.7% was removed by ISB, and 41% was either in the water column, degraded or in the sediments (30% shallower than 40 m and 11% below 40 m).

Without inclusion of SSDI in the model, ~96.4% of the oil surfaced (Table 2). Since in the base case during May–July, the fraction of oil remaining subsea averaged 11% (range 8–13%), SSDI reduced the amount of oil surfacing by 7% on average. Overall, SSDI reduced the total mass of volatiles (C5–C10) evaporating by ~13%. Application of dispersant at the water surface dispersed ~3.7% of the released oil into the water column. Modeled without surface dispersant application and ISB, about 2% more of the oil either went ashore or evaporated, and about 1% less degraded by the end of August 2010 (Table 1).

In the base case model, ~15,000 MT (2.7%) of the spilled oil mass was removed by ISB. This estimate is about one third of the estimate

Table 1
Modeled mass balance of total oil (C5+) on 31 August 2010, as percent of total oil spilled, for simulations assuming the potential range of initial droplet size distributions and for a simulation assuming no SSDI was performed.

Modeled droplet size distribution	% Atmosphere	% Surface	% Burned	% Ashore	% Sediment	% Water column	% Degraded	% Out of domain[a]	% Water column + % degraded + % out of domain
Spaulding et al. (2017) bimodal (base case)[b]	41.4	0.02	2.7	15.4	0.40	5.4	31.0	4.0	40.4
Spaulding et al. (2017) assuming low dispersant effectiveness[b]	44.5	0.03	2.6	16.4	0.51	5.2	26.9	4.1	36.2
Spaulding et al. (2017) assuming high dispersant effectiveness[b]	39.5	0.02	2.7	15.6	0.40	5.8	32.3	3.9	42.0
Spaulding et al. (2017) assuming no SSDI[c]	45.0	0.02	2.6	16.2	0.39	5.4	26.5	4.2	36.1
Spaulding et al. (2017) assuming no dispersant and no burning[d]	45.8	0.05	0.0	18.6	0.36	6.09	25.2	4.3	35.6

[a] Oil and components moving out of the model grid ("out of domain") were in the water column and would eventually biodegrade.
[b] Removal by in situ burning and surface dispersant included in model.
[c] Assuming no SSDI, but removal by in situ burning and surface dispersant activities included in model.
[d] Assuming no SSDI, and removal by in situ burning and surface dispersant were not included in model.

Table 2
Modeled percentage of total oil (C5+) mass remaining below the indicated water depths and ultimately biodegrading in the water column or reaching the sediments, for simulations assuming various daily-varying initial droplet size distributions from Spaulding et al. (2015, 2017).

Modeled droplet size distribution	% Below 900 m	% Below 200 m	% Below 40 m	% 200 m–900 m	% 40 m–200 m
Bimodal (base case)	5.3	10.0	10.7	4.7	0.7
Assuming low dispersant effectiveness	2.1	4.8	5.3	2.7	0.5
Assuming high dispersant effectiveness	5.8	12.3	13.3	7.3	1.0
Assuming no subsea dispersant	1.4	3.3	3.6	2.2	0.3

made by Mabile and Allen (2010), based on observed burn areas, burn times and an assumed 3 mm/min burn rate. The model predicted that there was insufficient oil thicker than the assumed minimum threshold (based on collection booming) to meet the Mabile and Allen burn volume estimates on all burn dates.

Mechanical removal was not simulated because quantitative estimates of the amounts of oil removed by location and over time were not available. Lehr et al. (2010) estimated that a total of about 2–5% of the spilled oil was skimmed, assuming 10–40% of recovered liquids were oil. As burning was limited by the amount of thick floating oil while environmental conditions were appropriate, inclusion of mechanical removal in the model would also have been limited during the same time periods, such that total removal (burning plus mechanical) would have been approximately the same as the modeled removal by burning.

Table C-8 (Appendix C) provides the mass balance of the oil pseudo-components on 31 August 2010 for the model simulation assuming the Spaulding et al. bimodal DSD. The results (summarized in Table 3) were that the Volatile Organic Compounds (VOCs: C5-C10 hydrocarbons, i.e., MAHs including BTEX, soluble alkanes and other aliphatics with boiling points <180 °C) mostly evaporated from surfaced oil, with the remaining mass dissolving prior to oil surfacing and then biodegrading in the water column. Table 4 shows that 80% of benzene was dissolved in the water column, and only 20% evaporated; whereas less soluble VOCs ranged up to 21% dissolved and 79% evaporated. By way of comparison, during the 1979 IXTOC I blowout in 60 m of water, Payne et al. (1980) also observed that the majority of the benzene released with the oil dissolved, with the other volatile aromatics and aliphatics volatilizing from the water or the oil phase after reaching the water surface. About 55% of the semi-volatile PACs evaporated, while most of the remaining PACs dissolved and ultimately degraded in the water column (Table 3). The percentages of the released oil pseudo-components retained below 40 m are in Table C-9 (Appendix C, SI), and the VOC

Table 4
Modeled percentage of spilled VOC mass dissolving below the indicated water depths and ultimately biodegrading in the water column, or surfacing and evaporating, assuming the bimodal droplet size distribution from Spaulding et al. (2017).

Pseudo-component	% Below 900 m	% Below 200 m	% Below 40 m	% Evaporated
Benzene	52	77	80	20
Toluene	34	50	53	47
Ethylbenzene & xylenes	26	35	37	63
C3-benzenes	21	27	28	71
Soluble alkanes (C5–C10)	14	20	21	79
Total VOCs	14	21	22	78

Table 3
Modeled mass balance on 31 August 2010, as percentage of spilled mass for groups of pseudo-components and for total oil (C5+), for the base case using the bimodal droplet size distribution from Spaulding et al. (2017).

Pseudo-components	% Atmosphere	% Surface	% Burned	% Ashore	% Sediment	% Water column	% Degraded	Out of domain
BTEX (AR1)	48.4	0.000	0.0	0.0	0.0	0.00	51.6	0.00
MAHs (AR2 + AR3)	73.4	0.000	0.0	0.0	0.0	0.00	26.6	0.00
PACs (PAHs & cyclic aromatics)	55.2	0.000	0.1	0.7	0.2	0.07	43.8	0.17
Aliphatics: C5–C10 (AR9 + AL1 + AL2)	81.3	0.000	0.0	0.0	0.0	0.00	18.7	0.00
Aliphatics: C11–C16 (AL3 + AL4 + AL5)	70.2	0.000	0.2	0.0	0.0	0.30	28.9	0.35
Aliphatics: C17–C23 (AL6 + AL7 + AL8)	53.0	0.004	1.5	4.6	0.1	1.50	37.5	2.14
Residual (C24+)	0	0.057	6.2	37.3	0.9	13.10	34.1	9.01
Total VOCs (AR1 + AR2 + AR9 + AL1 + AL2)	78.2	0.000	0.0	0.0	0.0	0.00	21.8	0.00

results are summarized in Table 4. Just over half the benzene and one third of the toluene dissolved in the deep plume and considerable fractions of these compounds dissolved before the rising oil droplets reached the water surface.

After 28 April 2010, >90% of the BTEX in the water column was in the dissolved form. For other pseudo-components, the percentage in the dissolved phase varied over the release period due to changing DSD and the amount of surfaced oil that entrained (Fig. C-15, Appendix C). Relatively low percentages of mass in the dissolved phase during April, early May and on June 3 followed periods when SSDI was not used. In the model, evaporation of VOCs occurred within an hour after oil surfacing. Thus, subsequent entrainment of surfaced oil did not result in consequential concentrations of dissolved BTEX or other VOCs in surface waters.

3.3.2. Comparisons to literature estimates

Early analyses of the mass balance (or "budget") for the DWH spill were based on partial information and expert opinion (Camilli et al., 2010; Lehr et al., 2010; McNutt et al., 2012b; Reddy et al., 2012) or used atmospheric VOC measurements made above and downwind of the surfacing oil on 8–10 June 2010 (Ryerson et al., 2012). Other discussions of the budget primarily reference these sources for their estimates (e.g., Boufadel et al., 2014; Joye, 2015; Joye et al., 2016; Passow and Hetland, 2016; Romero et al., 2017; Bracco et al., 2020; Passow and Overton, 2021). Further, clarification is needed whether a specific budget includes both the gas and oil, or the oil hydrocarbons above some carbon number (e.g., C5+).

Lehr et al.'s (2010) estimates, recalculated to exclude the amount recovered at the wellhead, were: skimmed (2–5%), burned (6–7%), dispersed in the water column (26–51%), evaporated or dissolved (24–30%), and other (13–35%), which included oil that was floating, ashore and in sediments. Comparisons to amounts skimmed and burned were discussed above. However, the purpose of the Lehr et al. (2010) report was to inform Incident Command during the spill response, and data were not available to improve estimate accuracy. Their objective was not to quantify the fate of oil (e.g., degradation). The water column estimates were based on assumed dispersant effectiveness for SSDI and surface applications, with a rough estimate of natural dispersion. Even so, those early estimates were not inconsistent with those of the present, much more detailed analysis.

In the base case model simulation, 11% of the released oil remained in waters below 40 m, falling within Valentine et al.'s (2014) estimated range of 4–31% being sequestered in the deep-sea. Daling et al. (2014) estimated dissolution loss during the ascent from depth to the surface included all the water-soluble hydrocarbons (~15% of the source oil), plus ~18% of the total PAH's (~0.2% of the source oil). The base case model estimates for the four PAC pseudo-components ranged from 8 to 23% remaining below 40 m, in agreement with Daling et al. (2014).

Ryerson et al. (2012) measured VOCs in the atmosphere in the area around the wellhead, estimating that, on June 10, 19–20% of the total *oil* hydrocarbon mass released to the environment was trapped in the deep plume, 8–9% was in the surface slicks near the wellhead, and 17.4–18.4% was evaporated; leaving ~54% unaccounted for in their analysis. They presumed that the missing fraction of oil was biodegraded, suspended in the water column other than in the deep intrusion layer, and/or on the seabed. The Ryerson et al. (2012) mass budget analysis has a number of sources of uncertainty, including that it depends on (1) an assumed oil mass released June 8–10 (to which an integration of measurements was compared), (2) an estimate of the total integrated DO anomaly from field samples by Kessler et al. (2011) and (3) Hazen et al.'s (2010) estimated ratios of alkanes to toluene in the plume phase versus in the leaking fluid phase (assumed to reflect the ratio of droplet to dissolved phase hydrocarbons – on the premise of the co-location of the dissolved and droplet phases). To the extent that droplets rose (or sank) out of the deep plume, preferentially leaving dissolved-phased hydrocarbons at depth (processes known to have occurred), the Ryerson et al. (2012) estimate of 19–20% of the oil mass being in the deep plume is an overestimate.

By comparison, SIMAP model estimates for all oil released by June 10 were ~19% in the water column (~4% below 40 m), 20% degraded (~6% below 40 m), 13% on the water surface, 39% in the atmosphere, and 7% ashore. By June 10, 90% of the oil released to date had surfaced and the other 10% was below 40 m. These results are consistent with Ryerson et al.'s (2012) estimates, given their likely over-estimation of the percentage in the deep plume and that they did not fully consider the cumulative fate from oil released earlier in the spill. We also note that Ryerson et al.'s estimates were based only on measurable compounds, whereas SIMAP's 39% evaporated also included mass measured in boiling cuts, but not measured by chemical analyses.

Based on their model analysis, assuming VMD = 1.3 mm from VDROP-J with mass in microdroplets <130 μm in diameter increased to 1.2% of the oil, Gros et al. (2017) concluded that 59% of the semi-soluble and non-soluble compounds (C10+) reached the sea surface on June 8. Approximating the DSD from Gros et al. (2017) and based on the rise times to the surface of the various droplet sizes calculated with SIMAP (Fig. C-7), 73.5% of the residual oil, which was released in >1 mm droplets, would surface by 11 h after a model initialization on June 8. Droplets >0.6 mm and >0.3 mm accounting for 93% and 97% of the residual oil would surface by 21 and 73 h, respectively. Thus, the time frame of the Gros et al. (2017) estimate influences the reported results, making comparisons difficult.

3.3.3. Oil sedimentation

Oil sedimentation occurred along with discharged olefin-containing Synthetic-Based drilling Muds (SBM) and sediments, particularly as part of the several unsuccessful top-kill activities during May 26–28, when ~30,000 bbl (4770 m^3) of SBM were released from the well into the water column (Stout and Payne, 2017). The footprint of SBM contamination was up to 10 cm thick within 2.3 km of the wellhead, comprising an area of ~6.5 km^2 (Stout and Payne, 2017). The oil mass associated with SBM was not included in spill volume estimates or in the mass balance herein.

In the deep-sea, the MC252 footprint on the sediment surface (~1 cm) extended to about 40 km from the well (Valentine et al., 2014; Stout and Payne, 2016a; Stout et al., 2016b, 2017; Stout and German, 2018; Babcock-Adams et al., 2017). The presented modeling includes sedimentation due to interactions with mineral SPM and bathtub ring impingement (Valentine et al., 2014; Stout et al., 2017) but does not include MOSSFA. A literature review was conducted to estimate the oil amount transported to sediments in marine oil snow (MOS). Typically, oil sedimentation via mineral-SPM interactions (variously called oil-mineral aggregates, OMAs, or oil-sediment aggregates, OSAs) becomes significant at >100 mg/L SPM (Boehm, 1987; Payne et al., 1987). Because mineral SPM concentrations are very low (<5 mg/L) in the offshore Gulf of Mexico (D'Sa et al., 2007; D'Sa and Ko, 2008; Salisbury et al., 2004), sedimentation of MC252 oil components identified in offshore sediments (Joye et al., 2011; Valentine et al., 2014; Chanton et al., 2015; Stout and Payne, 2016a, 2017; Stout et al., 2016b, 2017; Romero et al., 2017; Babcock-Adams et al., 2017; Passow and Stout, 2020) likely resulted from formation and settling of MOS (Passow et al., 2012; Ziervogel et al., 2014; Joye et al., 2014; Brooks et al., 2015; Passow, 2016; Daly et al., 2016; Romero et al., 2015, 2017; Babcock-Adams et al., 2017; Passow and Stout, 2020; Burd et al., 2020). Chemical analysis of offshore sediment samples showed patterns indicative of MOS sedimentation originating both from surfaced and subsea oil (Valentine et al., 2014; Romero et al., 2015, 2017; Stout et al., 2017; Stout and German, 2018; Passow and Stout, 2020).

Romero et al. (2017) estimated that $1.9 \pm 0.9 \times 10^4$ MT of hydrocarbons (>C9 measured saturated and aromatic fractions) from the DWH discharge settled in coastal, shelf and deep-sea sediments. Their estimate, that this represented ~21 ± 10% of the oil released to the environment, was based on the discharge volume in the USDC (2015)

decision, which was 77.3% of government estimate that we assumed. Relative to the government estimate of the spill volume, Romero et al.'s estimate corresponds to ~16 ± 8% of the oil released to the environment. Further, Romero et al. (2017) estimated 1253–2081 MT sedimented in coastal areas (not including 6729–35,560 MT in northern parts of Barataria and Terrebonne Bays), 277–395 MT on the continental shelf, and 1269–3213 MT in the deep-sea. In our model, it was assumed that oil reaching the coastline accumulated "on shore", and coastal oil/sediment dynamics were not simulated. Thus, much of the oil that would end up in coastal sediments was counted as on shore. The complexities of nearshore processes and petroleum sources other than the DWH spill contribute to uncertainties in the Romero et al. sedimentation estimates for coastal waters. Romero et al.'s (2017) estimates for sedimented mass for the shelf and deep-sea (which settled as part of MOS), accounting for the fraction of the C9+ compounds in the oil actually measured (20.9% by their estimate), amount to 1.3–3.1% of the 554,000 MT of C5+ oil released to the environment.

Estimates of excess (MC252) hopane in the sediments in 2010/2011 at depths of ~900–1700 m within 40 km of the wellhead made by Valentine et al. (2014) and Stout et al. (2017) were 1.8 ± 1.0 MT and 2.00–2.26 MT, equivalent to 4.7 ± 2.5% and 5.2–5.9%, respectively, of the released hopane (based on 68.8 mg hopane/kg oil, Stout et al., 2017; 554,000 MT oil released). Chanton et al. (2015) estimated an equivalent of 0.5 to 9.1% (best estimate 3.0–4.9%) of the discharged oil (based on ^{14}C in surface sediments) was in offshore sediments, a comparable range.

Based on forensic analysis of sediment trap samples from 58 km northeast of the well (400–450 m water depth), Stout and German (2018) estimated at least ~0.71 MT of hopane (1.9% of the hopane spilled) settled in MOS from surfaced oil. Of this, 7–11% was included in the deep-sea sedimented hopane estimate by Stout et al. (2017). Stout and German (2018) provided an updated estimate that 2.02–2.14 MT of hopane settled in MOS on the shelf and offshore in an area of 7600 km^2, and that 33–35% of the MOS settled from the surface and 65–67% originated from the deep plume. The average ratio of TPAH50 (sum of 50 PAHs considered by DWH Trustees (2016, Stout et al., 2017)) to hopane in the sediment traps during the active release period when surface-derived MOS settled was 6.1 (Stout and German, 2018), whereas in fresh oil it was 175 (Stout, 2015a). Thus, the oil in MOS from the surface was highly weathered residual oil, containing 3.5% of the original TPAH50 and none of the soluble compounds or volatiles. As hopane was 0.02% of the residual fraction, the 0.66–0.75 MT of hopane in MOS originating from surfaced oil represented 3645–4142 MT of settled oil, which was 0.7% of the oil released to the environment.

Sediment trap samples from 1400 m depth to 6.5 km southwest of the wellhead (Yan et al., 2016) indicated the oil in MOS at that depth was highly weathered. A relatively large pulse of MOS, collected 25 August–4 September 2010, had 9.3 times as much TPAH50 as hopane (Passow and Stout, 2020), indicating 5.3% of the original TPAH50 remained. This MOS pulse, which closely followed a phytoplankton bloom reported by Hu et al. (2011), contained high concentrations of diatom frustules, suggesting sinking phytoplankton marine snow scavenged oil droplets from the deep plume and carried them to the sea floor (Passow and Stout, 2020). Most of the compounds in pseudo-components AL1 to AL8 had biodegraded in the MOS captured by the 1400-m sediment trap (Passow and Stout, 2020), and in sediment samples taken >1.6 km from the well (Brakstad et al., 2018). Thus, ~40% of the original C5+ oil remained with the hopane in the MOS in the deep plume, and MOSSFA originating in the deep plume totaled 7558–8240 MT, representing 1.4–1.5% of the oil released to the environment. As the modeled amount of oil retained in the deep plume ranged from 11,080–33,230 MT (2–6% of the released oil), these estimates are in reasonable agreement.

While surface-derived MOS flux occurred during the period of active oil release (Stout and German, 2018), oil accumulated in the deep-sea sediments throughout the fall of 2010 and into 2011 (Yan et al., 2016; Passow and Stout, 2020). Babcock-Adams et al. (2017) found higher concentrations of petroleum biomarkers in deep-sea sediments in September 2010 relative to May 2010, followed by a peak in late November 2010 at stations near the well, concluding that most of the sedimentation did not occur during or immediately after the blowout. Thus, much of the MOS sedimentation from the deep plume occurred after 31 August 2010 (until July 2011), whereas the surface-derived MOSSFA occurred during the simulated period. This suggests that by not including MOSSFA in the model, ~0.7% of the oil counted as being in surface waters sedimented as part of surface-derived MOS.

Stout and Payne (2016b) estimated that 17.6% of burned oil formed residues (lumps and flakes) that sank to the seafloor. Based on the model-estimated 2.7% of the oil mass burned, ~0.5% of the spilled oil settled as burn residues. These residues likely were not present in sediment traps or samples.

In summary, based on the Stout and German (2018) and Passow and Stout (2020) analyses, and correcting for "oil" composition on the sea floor relative to hopane that was used to make the estimates, 2.1–2.2% of the 554 thousand MT of C5+ oil released settled via MOS on the shelf and in the deep-sea; ~0.7% from the surface and 1.4–1.5% originated from the deep plume. By 31 August 2010, modeled OSA sedimentation amounted to 0.4–0.5% of the oil released to the environment. MOS and OSA sedimentation on the shelf and in the deep-sea totaled ~1.2% by 31 August 2010, and ~2.6% of the spilled oil by 2011. Sedimented burn residues accounted for another ~0.5% of the spilled oil. Thus, ~3.1% of the spilled oil reached shelf and deep-sea sediments. This estimate is consistent with Romero et al.'s (2017) estimates for sedimented mass on the shelf and in the deep-sea, which were equivalent to 1.3–3.1% of the spill oil, and with Chanton et al.'s (2015) best estimate of 3.0–4.9% of the discharged oil in offshore sediments.

3.4. Comparison of model results to observational data

3.4.1. Surface oil

3.4.1.1. Amount of floating oil. Fig. 4 compares the modeled floating oil volume over time for the base case (using the Spaulding et al. bimodal DSD) with estimates based on interpretation of remote sensing imagery. The average oil thickness estimates for MVIS, MTIR, and Landsat TM are uncertain, being based on representative values within broad ranges (Table C-7, Appendix C). The SAR estimates developed by MacDonald et al. (2015) were more narrowly quantified based on field data, albeit they are estimates of average thickness for highly variable oil coverages. From 1 May to 31 July 2010, the modeled floating oil volumes (not including the water in emulsions) averaged 27,100 m^3 (26,500 MT), whereas the SAR-based estimates averaged 25,900 m^3. The comparisons in various time intervals show good agreement, well within ±one standard deviation, indicating the Spaulding et al. (2015, 2017) bimodal DSD and SIMAP model produced reasonable results (Table 5).

The model-predicted floating oil mass increased to a maximum of ~62,000 MT on June 3, then declined to ~127 MT on August 31 (Fig. 3). Floating oil was "visible" via remote sensing until the August 9th SAR observation (MacDonald et al., 2015), when the model predicted 6200 MT. SAR and other imagery could not detect areas of weathered oil residuals, only fresh oil, emulsions and continuous sheens (Garcia-Pineda et al., 2009, 2013a, 2013b; Hu et al., 2009; Leifer et al., 2012; Svejkovsky et al., 2012, 2016; MacDonald et al., 2015). Over time, floating oil entrained into the water or became weathered residuals (defined as when pseudo-components AR1–AR9 and AL1–AL8 summed to <1% of oil mass), assumed awash in the wave mixed layer of the water column. By August 31, 61% of the water column mass was in the form of weathered residuals, either in surface waters or in the deep sea. These residuals would have been the source for MOS in the fall of 2010.

Approximating the DSD from Gros et al. (2017) (see French-McCay et al. (2021b) and accounting for evaporation and re-entrainment,

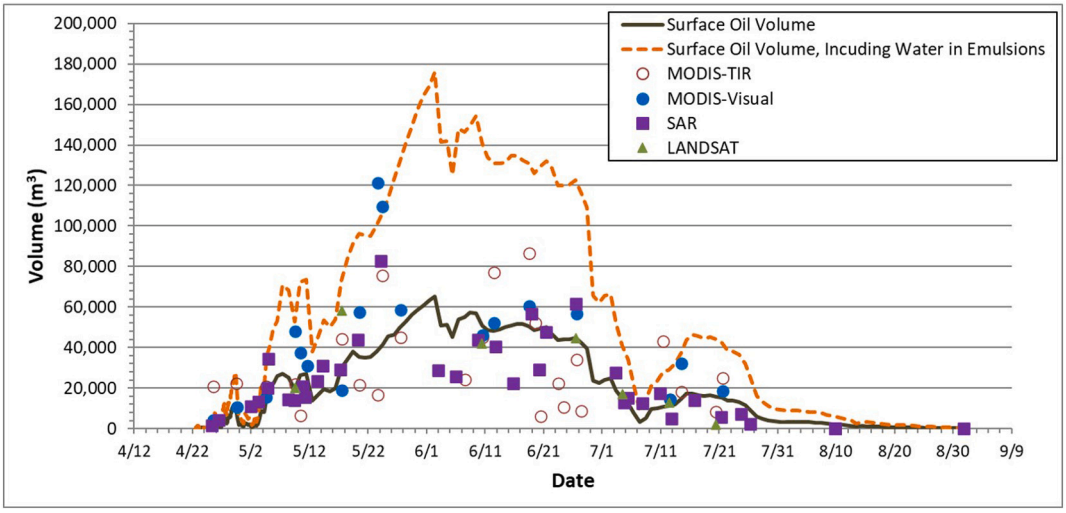

Fig. 4. Model-predicted (base case) floating oil volumes, as oil only and volume including water in emulsions, compared to estimated volumes based on remote sensing data.

Table 5
Modeled (mean over the indicated time) and remote sensing-based estimates (based on SAR observations) of surface floating oil.

Dates in 2010	Modeled oil (MT)	Modeled oil (m^3)	Model oil with water in emulsions (m^3)	Oil based on SAR (m^3)		
				Mean	Standard deviation	# Observations
April	2890	3000	6600	2800	2000	2
May	22,700	23,300	59,700	27,200	19,600	13
June	47,400	48,300	130,200	39,600	14,100	9
July 1–15	12,800	13,100	34,500	15,100	7500	6
May 1–July 15	29,200	29,800	78,580	28,600	17,800	28
July	11,900	12,200	32,700	11,900	7500	10
May 1–July 31	26,500	27,100	71,500	25,900	18,200	32

during June 8–10 the floating oil amounted to 32–34% of the released oil assuming the ~Gros et al. (2017) DSD and 13–15% assuming the Spaulding et al. (2015, 2017) bimodal DSD. Thus, the ~Gros et al. (2017) DSD resulted in ~2.4 times as much floating oil as the Spaulding et al. (2017) bimodal DSD, an amount higher than indicated by the remote sensing data (Fig. 4).

3.4.1.2. Weathering state. Stout and Payne (2016b) and Stout et al. (2016a) analyzed the weathering state of 62 floating oil samples collected May–July 2010, finding that by the time the oil reached the water surface, it had lost most of the mass below C8 (i.e., BTEX, AR1, and soluble alkanes, AR9). Freshly surfaced oil did contain some measurable BTEX and soluble alkanes (Stout et al., 2016a). However, evaporation quickly depleted the mass content up to C13 (i.e., alkanes to n-C13 and 1- to 2-ring aromatics) while oil was within 10 km of the wellhead. Ryerson et al. (2011) found no detectable VOCs in the atmosphere outside of a narrow plume extending ~10 km downwind of the wellhead. The model predicted consistent results; floating oil within 10 km of the well was >95% depleted of compounds up to C13, and >98% depleted of compounds up to C10.

TPAH50 (corresponding to pseudo-components AR5 to AR8) in floating oil samples collected <10 km from the wellhead were depleted 12–91%. Freshly surfaced oil was ~12% depleted in TPAH50, while continual re-supply of surfacing oil and evaporation reduced the average to 54 ± 20%. Samples collected 10–75 km from the well, exhibited 85 ± 14% depletion of TPAH50 (Stout et al., 2016a). The model predicted consistent TPAH50 results with these floating oil samples (Table 6). Freshly surfaced oil within 10 km of the wellhead averaged 7% TPAH50 depletion (range 1–16%) during June 2010, as compared to 12% for the sample taken on June 16th at 2 km from the well.

Table 6
Modeled percentage of TPAH50 in floating oil, assuming the bimodal droplet size distribution from Spaulding et al. (2017), compared to analyses of 60 floating oil samples taken 10 May to June 20, 2010 from Stout et al. (2016a).

Source	Distance	May	June	Overall
Samples	<10 km	54 ± 15	53 ± 35	54 ± 20
Samples	10–75 km	86 ± 16	83 ± 8	85 ± 14
Model	<2 km	20.8	26.0	22.9
Model	2–4 km	38.0	48.4	42.0
Model	4–10 km	50.2	64.4	54.2
Model	<10 km	46.1	56.3	49.3
Model	All	73.9	80.8	77.4

While photo-oxidation is an important weathering process for floating oil (Ward et al., 2018; Ward and Overton, 2020), the fate of photoproducts resulting from photo-oxidation was not quantified herein. Research is needed to characterize both the production rates and the properties of the photoproducts to quantify their dissolution, biodegradation, and fate.

3.4.2. Atmospheric emissions

The modeled mass flux to the atmosphere (Fig. 5) varied with changing wind conditions, as the DSD changed with varying SSDI applications (Fig. B-3, Appendix B), and as the amount of oil released to the environment decreased (Fig. B-1, Appendix B). The atmospheric flux of VOCs, including soluble pseudo-components (BTEX, C3-benzenes), decreased throughout the spill as SSDI became more effective (Fig. 5; Figs. C-16 and C-17, Appendix C). Semi-soluble and non-soluble volatile emissions peaked during periods when droplet sizes were relatively large (i.e., when there was no SSDI). Table 3 summarizes the evaporated

mass percentages for the volatile and semi-volatile pseudo-components. Table 7 lists the average VOC flux (MT/hour), and percent reductions from the model case assuming no SSDI, for specific periods. VOC emissions became negligible just after the release stopped. VOC emissions were reduced by 4% in May, 23% in June, and 26% in the first half of July (uncertainty ranges in Table 7). The average reduction in VOC emissions during June 3–July 10, when SSDI was relatively consistently applied, was 26%.

Based on shipborne and airborne measurements during 8–10 June 2010, Ryerson et al. (2012) estimated that 460 ± 230 MT of hydrocarbons evaporated on June 10. The uncertainty (± 50%) was attributed to uncertainties in the integration of atmospheric plume hydrocarbon data from samples taken along the transects flown. Of the 460 MT/day (Table 8), 258 MT/day were of measurable hydrocarbons up to C11, with <n-C4 alkanes negligible. C6 through C11 aromatic compounds (BTEX, C3-benzenes and naphthalene being measured) contributed 45 MT/day to this flux (Ryerson et al., 2011, 2012). Ryerson et al. (2012) estimated (modeled) the evaporated flux of unmeasured semi-volatile alkanes >n-C11 (202 MT/day) using the volatility distribution of the oil mixture determined from the chemical composition and evaporation measurements in laboratory studies (de Gouw et al., 2011).

The ranges of modeled atmospheric flux estimates for June 10, assuming various DSDs, overlap with the Ryerson et al. (2012) uncertainty ranges. The modeled base-case estimates are higher than the Ryerson et al. estimates for ≤C11 volatiles, but consistent for C11+ semi-volatiles (Table 8). The Ryerson et al. (2012) ≤C11 flux was underestimated to the extent some of the evaporating mass was missed, either during sampling or because only some of the modeled compounds were measured in field samples. Alternatively, the model could have underestimated dissolution of the volatiles prior to surfacing, due to the assumed DSD. The high-effectiveness DSD (100% effectiveness) leads to the lowest atmospheric VOC flux, which agrees with the Ryerson et al. (2012) estimates, suggesting more dispersant effectiveness (smaller droplets) than either the base case or the ~Gros et al. (2017) DSD. However, that extreme case is unlikely as it assumed the subsea dispersant applications were 100% effective on the oil in the oil and gas plume, suggesting Ryerson et al. (2012) instead under-estimated the atmospheric flux.

4. Summary and conclusions

4.1. DSD model

The analyses discussed above compare model results to field data related to floating oil (amounts and weathering states) and atmospheric emissions. In the companion paper (French-McCay et al., 2021b), model results and sample chemistry data from the deep plume are analyzed in detail, using fractionation indices (Reddy et al., 2012; Ryerson et al., 2012; Gros et al., 2017) to evaluate chemical partitioning between deep and surface waters assuming the potential range of DSDs released from the nearfield. These comparisons validated the modeled oil fate and mass balance.

Field evidence and model calculations support the presence of both large droplets (VMD > 1 mm) and small droplets (VMD < 300 μm) when SSDI was performed, as well as the production of small droplets during May via the releases though the kink holes. Observations of the dispersant treatment techniques, and the complex release conditions during June 4–July 10 when Top Hat #4 and the recovery pipe were in place, disrupting the buoyant plume dynamics, indicate the partial-treatment bimodal DSD described by Spaulding et al. (2017) is the most realistic model of those examined. In addition, dispersant-induced tip-streaming (Zhao et al., 2017b; Gros et al., 2017; Boufadel et al., 2020), or some other mechanism resulting in the formation of micro-droplets, may have coincided with the bulk of the oil present in a DSD of larger droplets (Boufadel et al., 2018).

4.2. Effectiveness of subsea dispersant use

The percentage of oil dispersed and remaining subsea varied from 8 to 13% during the SSDI usage period, limited by the low amounts of dispersant applied per oil volume (<1%) and the variable dispersant application effectiveness, as well as time intervals without SSDI. On average over the entire spill, SSDI reduced the oil mass surfacing by ~7.1% and increased mass retained in the water column by ~3.9% at depths >900 m, ~2.5% between 200 and 900 m deep, and 0.4% between 40 and 200 m (Table 2). The other 0.9% was dispersed in surface waters (<40 m).

From 1 May to 31 July 2010, the (base case) model-predicted floating oil averaged 26,500 MT. Assuming no subsea dispersant use, the model predicted an average of 29,200 MT of floating oil would have been present in that period. Thus, on average, there was 9% less oil floating during May–July because of the subsea dispersant applications.

Because weathering processes (dissolution and biodegradation) are faster for smaller oil droplets due to their higher surface area per unit volume (see experimental evidence in Brakstad et al., 2015), and since smaller droplets rise more slowly, much more dissolution and biodegradation occurred at depth when droplet size was reduced by inclusion of SSDI. Consequently, SSDI reduced the VOC content of surfacing oil,

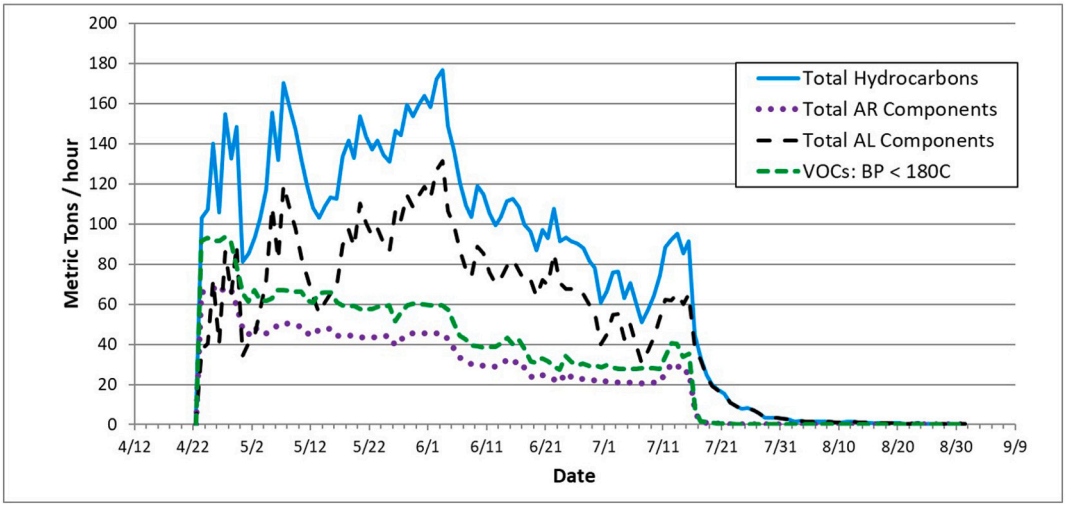

Fig. 5. Emissions of Volatile Organic Compounds (VOCs) and semi-volatile compounds to the atmosphere for the base case assuming the bimodal droplet size distribution.

Table 7
Average mass flux (MT/hour) of VOCs to the atmosphere, and percent reduction from the model assuming no SSDI, modeled using the droplet size distributions from Spaulding et al. (2017). (Base case is the bimodal droplet size distribution.)

Case and metric	April	May	June	July 1–15	July 16–31	May 1–July 15	June 3–July 10	June 8–10
Base case (MT/hour)	70.0	62.2	38.9	31.0	0.5	49.5	34.6	39.0
No SSDI (MT/hour)	70.0	65.0	50.6	42.1	0.0	56.6	46.7	53.5
% VOC reduction for base case	0	4.4	23	26	−100	13	26	27
% VOC reduction for low SSDI effectiveness	0	1.6	10	13	−100	5.5	12	7.2
% VOC reduction for high SSDI effectiveness	0	9.4	42	59	−100	25	51	48

Table 8
Atmospheric emissions for June 10, as estimated by Ryerson and predicted by the model, assuming the three potential droplet size distributions from Spaulding et al. (2015, 2017a) and approximating the droplet size distribution from Gros et al. (2017).

Compound group	Ryerson et al. (2011, 2012); MT/day	Model – base case (high – low effectiveness DSD); MT/day	Model – assuming ~ Gros et al. (2017) droplet size distribution; MT/day
n-C4 to n-C11 alkanes	213 ± 107	571 (331–772)	790
BTEX, C3-benzenes and naphthalene	45 ± 23	80 (10–61)	64
Subtotal (C4 to C11 compounds)	258 ± 129	651 (341–833)	854
C12 to C16 alkanes	202 ± 101	217 (211–298)	281
Total (C1 to C16 compounds)	460 ± 230	868 (332–1131)	1135

and so reduced the evaporative flux of VOCs. SSDI reduced VOC evaporation (i.e., BTEX, C3-benzenes, and C5–C10 alkanes) by ~4% in May 2010 and by ~26% during 3 June–10 July 2010 (Table 7) because the DSD was shifted to smaller droplet sizes. Thus, the SSDI applications were increasingly effective over the course of the spill in reducing VOC exposures in the immediate area of the wellhead (since VOCs evaporated within an hour of the large untreated droplets surfacing near the well). Our estimates are corroborated by analyses by Gros et al. (2017), who concluded that VOC (C1–C9) emissions were decreased 28% by SSDI during June 2010, based on nearfield model calculations for 8 June 2010. Our model estimated that SSDI decreased the VOC (C5–C10) flux to the air by 27% during 8–10 June 2010.

4.3. Oil mass balance

Based on the model results, and supported by comparisons to field observations, our best estimates of the oil mass balance are that of the spilled oil (C5+), ~41% evaporated, ~15% came ashore and ~ 3% was removed mechanically or by in situ burning. The other 41% of the oil was in the water column on 31 August 2010, where it ultimately degraded or settled to the sediments. The uncertainty range is ±10% of these estimates based on the range of potential DSDs. Nearly three quarters of the oil in the water column (30% of the released oil) had first surfaced and re-entrained by natural and dispersant-facilitated dispersion or by break up into particulate oil residuals. The other ~11% of the released oil, included 5% that entered (by dissolving or as microdroplets) the deep plume where it biodegraded or sedimented in the deep sea, and ~6% that dissolved and biodegraded in midwaters between 900 m and 40 m (5% between 900 and 200 m, 1% between 200 and 40 m). Biodegradation of the volatile and soluble fractions remaining below 40 m was largely complete by the end of August 2010.

We did not model nearshore sedimentation in coastal waters of oil that first reached shorelines. Some of the 15% of released oil coming ashore was cleaned up, and the remainder likely was incorporated into sediments near the shoreline. Our estimate is that ~3.1% of the C5+ oil settled on the shelf and in the deep sea, including ISB residues (~0.5%), MOS (~2.2%) and modeled settlement by OMA (~0.4%), leaving 38% in the water column by July 2011 (40% on 31 August 2010, adjusted downward for MOS). MOS and oil sedimentation has been discussed at length in the published literature (Passow et al., 2012; Fu et al., 2014; Joye et al., 2014; Chanton et al., 2015; Brooks et al., 2015; Passow, 2016; Passow and Ziervogel, 2016; Daly et al., 2016; Stout et al., 2016b, 2017; Romero et al., 2015, 2017; Babcock-Adams et al., 2017; Burd et al., 2020), with many concluding that the percentage accounted by MOS settlement was much higher than the ~2.2% we estimate based on analyses by Stout and German (2018) and Passow and Stout (2020; i.e., 0.7% from the surface and ~1.5% from the deep plume). Much of this discrepancy is reconciled when the fraction of the C5+ oil that settled is quantified (as opposed to assuming that if, for example, 5% of hopane settled, 5% of the released oil settled) and the total spill mass considered is the C5+ oil released to the environment (i.e., less the subsea recovery) based on the best estimates of daily oil volume released, that from McNutt et al. (2012a). Romero et al.'s (2017) estimates equate to ~1.3–3.1%, and Chanton et al.'s (2015) estimates equate to 3.0–4.9%, of the released oil settled on the shelf and in the deep-sea, corroborating our 3.1% estimate for shelf and deep-sea sedimentation.

The mass balance of the released oil by summer of 2011 (summarized in Fig. 6), adjusted for MOS settlement, was ~41% evaporated, ~15% ashore and in nearshore sediments (areas <10 m deep), ~3% burned or mechanically removed, ~38.4% in the water column (partially degraded; 29% shallower and 9.4% deeper than 40 m), and 2.6% sedimented by MOS and OMA deeper than 10 m. The oil fate and mass balance largely reflected the oil composition and bulk properties, the release depth, environmental conditions, and the DSD predicted based on oil and gas flow rates, release locations and configurations, and dispersant applications at the wellhead. The mass balance was verified by detailed analysis of observations (herein) and chemistry sample data (in companion paper, French-McCay et al., 2021b). For the most part, our estimates compare favorably with other published estimates when differences in components are considered (e.g., oil only versus oil and gas) and assumed release amounts are reconciled. Our modeling analyses were not calibrated or adjusted to fit observational data, allowing the model and results to be validated. As such, the oil mass balance results are robust.

Appendices A – C. Supplementary data. Supplementary data to this article can be found online at https://doi.org/10.1016/j.marpolbul.2021.112681.

CRediT authorship contribution statement

Deborah P. French-McCay: Conceptualization, Methodology, Investigation, Formal analysis, Validation, Writing – original draft, Writing – review & editing, Supervision, Project administration. **Katherine Jayko:** Methodology, Software, Validation, Data curation. **Zhengkai Li:** Methodology, Investigation, Formal analysis. **Malcolm L. Spaulding:** Conceptualization, Methodology, Formal analysis, Validation, Supervision, Writing – original draft, Writing – review & editing. **Deborah Crowley:** Methodology, Formal analysis, Software, Visualization. **Daniel Mendelsohn:** Conceptualization, Methodology,

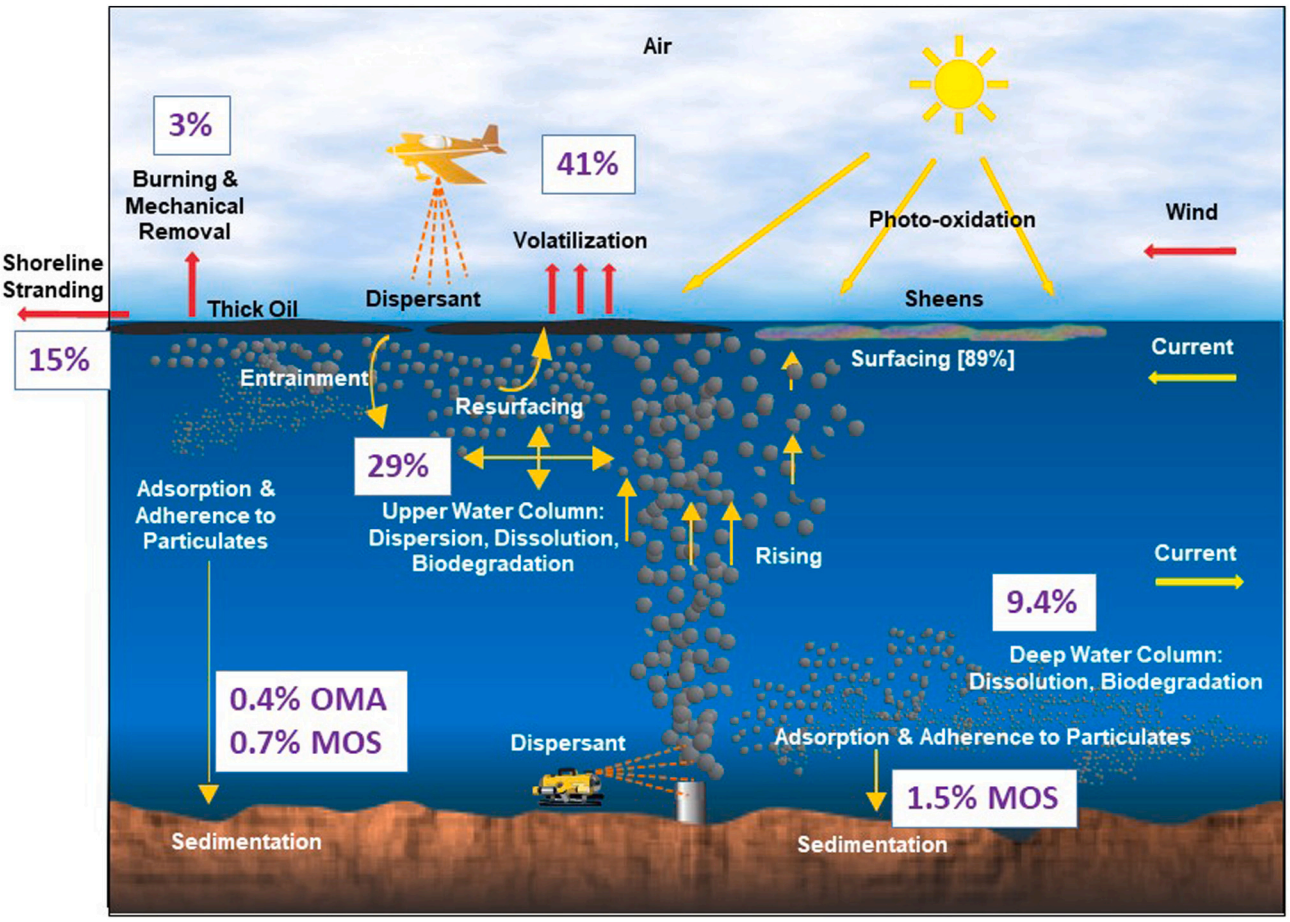

Fig. 6. Oil fate and mass budget for the DWH oil (C5+) by July of 2011.

Investigation, Formal analysis, Software. **Matthew Horn:** Methodology, Investigation, Validation, Data curation, Visualization, Writing – original draft. **Tatsusaburo Isaji:** Formal analysis, Software. **Yong Hoon Kim:** Investigation, Formal analysis, Validation, Data curation. **Jeremy Fontenault:** Formal analysis, Visualization. **Jill J. Rowe:** Supervision, Project administration.

Declaration of competing interest

The authors declare that they have no known competing financial interests or personal relationships that could have appeared to influence the work reported in this paper.

Acknowledgements

This work was supported in part by the National Oceanic and Atmospheric Administration Damage Assessment, Remediation and Restoration Program (NOAA Contract No. AB133C-11-CQ-0050) and by the US Department of the Interior, Bureau of Ocean Energy Management, Environmental Studies Program, Washington, DC (BOEM Contract Number M11PC00028). The opinions expressed by the authors are their own and do not necessarily reflect the opinion or policy of the U.S. Government. Any use of trade, firm, or product names is for descriptive purposes only and does not imply endorsement by the U.S. Government.

The authors acknowledge the contributions of Cheryl Morse (RPS) for model code preparation, testing and debugging and Andrew Menton (RPS) for compiling surface response activity data. Eileen Graham and Andrew Bird, formerly of RPS, contributed to data collection, quality control, and compilation efforts. Hilary Robinson and Missy Gloekler (RPS) provided valuable comments upon reviewing drafts of this manuscript.

References

Adams, E.E., Socolofsky, S.A., Boufadel, M., 2013. Comment on "Evolution of the Macondo well blowout: simulating the effects of the circulation and synthetic dispersants on the subsea oil transport". Environ. Sci. Technol. 47 (20), 11905. https://doi.org/10.1021/es4034099.

Adcroft, A., Hallberg, R., Dunne, J.P., Samuels, B.L., Galt, J.A., Barker, C.H., Payton, D., 2010. Simulations of underwater plumes of dissolved oil in the Gulf of Mexico. Geophys. Res. Lett. 37, L18605 https://doi.org/10.1029/2010GL044689.

Aman, Z.M., Paris, C.B., May, E.F., Johns, M.L., Lindo-Atichati, D., 2015. High-pressure visual experimental studies of oil-in-water dispersion droplet size. Chem. Eng. Sci. 127 (0), 392–400. https://doi.org/10.1016/j.ces.2015.01.058.

Babcock-Adams, J.P. Chanton, Joye, S.B., Medeiros, P.M., 2017. Hydrocarbon composition and concentrations in the Gulf of Mexico sediments in the 3 years following the Macondo well blowout. Environ. Pollut. 229, 329–338. https://doi.org/10.1016/j.envpol.2017.05.078.

Bandara, U.C., Yapa, P.D., 2011. Bubble sizes, breakup, and coalescence in deepwater gas/oil plumes. J. Hydraul. Eng. ASCE 137 (7), 729–738. https://doi.org/10.1061/(asce)hy.1943-7900.0000380.

Boehm, P.D., 1987. Transport and transformation processes regarding hydrocarbon and metal pollutants in offshore sedimentary environments. In: Boesch, D.F., Rabalais, N. (Eds.), Long-term Environmental Effects of Offshore Oil and Gas Development. Taylor and Francis, London, New York, pp. 233–286.

Boufadel, M.C., Nasab, A.-A., Geng, X., Galt, J., Torlapati, J., 2014. Simulation of the landfall of the Deepwater Horizon oil on the shorelines of the Gulf of Mexico. Environ. Sci. Technol. 48, 9496–9505. https://doi.org/10.1021/es5012862.

Boufadel, M.C., Gao, F., Zhao, L., Özgökmen, T., Miller, R., King, T., Robinson, B., Lee, K., Leifer, I., 2018. Was the Deepwater Horizon well discharge churn flow? Implications on the estimation of the oil discharge and droplet size distribution. Geophys. Res. Lett. 45, 2396–2403. https://doi.org/10.1002/2017GL076606.

Boufadel, M.C., Socolofsky, S., Katz, J., Yang, D., Daskiran, C., Dewar, W., 2020. A review on multiphase underwater jets and plumes: droplets, hydrodynamics, and chemistry. Rev. Geophys. 58, e2020RG000703 https://doi.org/10.1029/2020RG000703.

Bracco, A., Paris, C.B., Esbaugh, A.J., Frasier, K., Joye, S.B., Liu, G., Polzin, K.L., Vaz, A. C., 2020. Transport, fate and impacts of the deep plume of petroleum hydrocarbons formed during the Macondo blowout. Front. Mar. Sci. 7, 764. https://doi.org/10.3389/fmars.2020.542147.

Brakstad, O.G., Nordtug, T., Throne-Holst, M., 2015. Biodegradation of dispersed Macondo oil in seawater at low temperature and different oil droplet sizes. Mar. Pollut. Bull. 93 (1–2), 144–152. https://doi.org/10.1016/j.marpolbul.2015.02.006.

Brakstad, O.G., Lewis, A., Beegle-Krause, C.J., 2018. A critical review of marine snow in the context of oil spills and oil spill dispersant treatment with focus on the Deepwater Horizon oil spill. Mar. Pollut. Bull. 135, 346–356. https://doi.org/10.1016/j.marpolbul.2018.07.028.

Brooks, G.R., Larson, R.A., Schwing, P.T., Romero, I., Moore, C., Reichart, G.-J., Jilbert, T., Chanton, J.P., et al., 2015. Sedimentation pulse in the NE Gulf of Mexico following the 2010 DWH blowout. PLoS One 10 (7), e0132341. https://doi.org/10.1371/journal.pone.0132341.

Burd, A.B., Canton, J.P., Daly, K., Gilbert, S., Passow, U., Quigg, A., 2020. The science behind marine-oil snow and MOSSFA: past, present, and future. Prog. Oceanogr. 187 (2020), 102398 https://doi.org/10.1016/j.pocean.2020.102398.

Camilli, R., Reddy, C.M., Yoerger, D.R., Van Mooy, B.A.S., Jakuba, M.V., Kinsey, J.C., Mcintyre, C.P., Sylva, S.P., Maloney, J.V., 2010. Tracking hydrocarbon plume transport and biodegradation at Deepwater Horizon. Science 330, 201–204. https://doi.org/10.1126/science.1195223.

Chan, G., Chow, A., Adams, E.E., 2015. Effects of droplet size on intrusion of sub-surface oil spills. Environ. Fluid Mech. 15 (5), 959–973. https://doi.org/10.1007/s10652-014-9389-5.

Chanton, J., Zhao, T., Rosenheim, B.E., Joye, S., Bosman, S., Brunner, C., Yeager, K.M., Diercks, A.R., Hollander, D., 2015. Using natural abundance radiocarbon to trace the flux of petrocarbon to the seafloor following the Deepwater Horizon oil spill. Environ. Sci. Technol. 49, 847–854. https://doi.org/10.1021/es5046524.

Chassignet, E.P., Srinivasan, A., 2015. Data Assimilative Hindcast for the Gulf of Mexico. US Dept. of the Interior, Bureau of Ocean Energy Management, p. 40. OCS Study BOEM 2015-035. https://espis.boem.gov/final%20reports/5479.pdf.

Chen, F.H., Yapa, P.D., 2002. A model for simulating deepwater oil and gas blowouts - part II: comparison of numerical simulations with "Deepspill" field experiments. J. Hydraul. Res. IAHR 41 (4), 353–365. https://doi.org/10.1080/00221680309499981.

Chen, F., Yapa, P., 2007. Estimating the oil droplet size distributions in deepwater oil spills. J. Hydraul. Eng. 133 (2), 197–207. https://doi.org/10.1061/(ASCE)0733-9429(2007)133:2(197).

Cooper, C., Adams, E., Gros, J., 2021. An evaluation of models that estimate droplet size from subsurface oil releases. Mar. Pollut. Bull. 163, 111932 https://doi.org/10.1016/j.marpolbul.2020.111932.

Crowley, D., Mendelsohn, D., Mulanaphy, N.W., Li, Z., Spaulding, M.L., 2014. Modeling subsurface dispersant applications for response planning and preparation. Int. Oil Spill Conf. Proc. 2014 (1), 933–948. https://doi.org/10.7901/2169-3358-2014.1.933.

Daae, R.L., Skancke, J., Brandvik, P.J., Faksness, L.-G., 2018. The sensitivity of the surface oil signature to subsurface dispersant injection and weather conditions. Mar. Pollut. Bull. 127, 175–181. https://doi.org/10.1016/j.marpolbul.2017.11.067.

Daling, P.S., Leirvik, F., Almås, I.K., Brandvik, P.J., Hansen, B.H., Lewis, A., Reed, M., 2014. Surface weathering and dispersibility of MC252 crude oil. Mar. Pollut. Bull. 87 (1–2), 300–310. https://doi.org/10.1016/j.marpolbul.2014.07.005.

Daly, K.L., Passow, U., Chanton, J., Hollander, D., 2016. Assessing the impacts of oil associated marine snow formation and sedimentation during and after the Deepwater Horizon oil spill. Anthropocene 1-1, 6. https://doi.org/10.1016/j.ancene.2016.01.006.

Davis, C.S., Loomis, N.C., 2014. Deepwater Horizon Oil Spill (DWHOS) Water Column Technical Working Group Image Data Processing Plan: Holocam, Description of Data Processing Methods Used to Determine Oil Droplet Size Distributions From In Situ Holographic Imaging During June 2010 on Cruise M/V Jack Fitz 3. Woods Hole Oceanographic Institution. MIT/WHOI Joint Program in Oceanography, 15 p. + Appendix. DWH-AR0047462.pdf. https://www.doi.gov/deepwaterhorizon/adminrecord.

Deepwater Horizon Natural Resource Damage Assessment Trustee Council (DWH Trustees), 2016. The Deepwater Horizon Oil Spill Final Programmatic Damage Assessment and Restoration Plan and Final Programmatic Environmental Impact Statement. National Oceanic and Atmospheric Administration, Office of Response and Restoration. http://www.gulfspillrestoration.noaa.gov/restoration-planning/gulf-plan/.

Diercks, A.R., Highsmith, R.C., Asper, V.L., Joung, D., Zhou, Z., Guo, L., Shiller, A.M., Joye, S.B., Teske, A.P., Guinasso, N., Wade, T.L., Lohrenz, S.E., 2010. Characterization of subsurface polycyclic aromatic hydrocarbons at the Deepwater Horizon site. Geophys. Res. Lett. 37, L20602, 1-6. https://doi.org/10.1029/2010GL045046.

Dietrich, J.C., Trahana, C.J., Howard, M.T., Fleming, J.G., Weaver, R.J., Tanakae, D.S., Yuf, L., Luettich Jr., R.A., Dawson, C.N., Westerink, J.J., Wells, G., Lu, A., Vega, K., Kubach, A., Dresback, K.M., Kolar, R.L., Kaiser, C., Twilley, R.R., 2012. Surface trajectories of oil transport along the northern coastline of the Gulf of Mexico. Cont. Shelf Res. 41 (1), 17–47. https://doi.org/10.1016/j.csr.2012.03.015.

Driskell, W.B., Payne, J.R., 2018a. Development and application of phase-specific methods in oiled-water forensic studies. In: Stout, S., Wang, Z. (Eds.), Oil Spill Environmental Forensics – Case Studies. Elsevier/Academic Press, pp. 289–321. ISBN: 978-O-12-804434-6.

Driskell, W.B., Payne, J.R., 2018b. Macondo oil in northern Gulf of Mexico waters – part 2: dispersant-accelerated PAH dissolution in the Deepwater Horizon plume. Mar. Pollut. Bull. 129, 412–419. https://doi.org/10.1016/j.marpolbul.2018.02.057.

D'Sa, E.J., Ko, D.S., 2008. Short-term influences on suspended particulate matter distribution in the northern Gulf of Mexico: satellite and model observations. Sensors 8, 4249–4261. https://doi.org/10.3390/s8074249.

D'Sa, E.J., Miller, R.L., McKee, B.A., 2007. Suspended particulate matter dynamics in coastal waters from ocean color: application to the northern Gulf of Mexico. Geophys. Res. Lett. 34, 6. https://doi.org/10.1029/2007GL031192.

ERMA, 2016. The ERMA® Deepwater Gulf Response Web Application. https://erma.noaa.gov/gulfofmexico/erma.html#/layers=3+10717+16023+17774+32237+32238+32239+32240&x=-89.48747&y=27.92566&z=6.4&panel=layer.

French-McCay, D.P., 2003. Development and application of damage assessment modeling: example assessment for the North Cape oil spill. Mar. Pollut. Bull. 47 (9–12), 341–359. https://doi.org/10.1016/s0025-326X(03)00208-X.

French-McCay, D.P., 2004. Oil spill impact modeling: development and validation. Environ. Toxicol. Chem. 23 (10), 2441–2456. https://doi.org/10.1897/03-382.

French-McCay, D.P., 2008. Modeling as a scientific tool in NRDA for oil and chemical spills. Int. Oil Spill Conf. Proc. 2008 (1), 1147–1151. https://doi.org/10.7901/2169-3358-2008-1-1147, 2008.

French-McCay, D., Whittier, N., Sankaranarayanan, S., Jennings, J., Etkin, D.S., 2004. Estimation of potential impacts and natural resource damages of oil. J. Hazard. Mater. 107 (1–2), 11–25. https://doi.org/10.1016/j.jhazmat.2003.11.013.

French-McCay, D.P., Jayko, K., Li, Z., Horn, M., Kim, Y., Isaji, T., Crowley, D., Spaulding, M., Decker, L., Turner, C., Zamorski, S., Fontenault, J., Shmookler, R., Rowe, J.J., 2015a. Technical Reports for Deepwater Horizon Water Column Injury Assessment – WC_TR14: Modeling Oil Fate and Exposure Concentrations in the Deepwater Plume and Cone of Rising Oil Resulting from the Deepwater Horizon Oil Spill. DWH NRDA Water Column Technical Working Group Report. Prepared for National Oceanic and Atmospheric Administration by RPS ASA, South Kingstown, RI, USA. September 29, 2015. Administrative Record no. DWH-AR0285776.pdf. https://www.doi.gov/deepwaterhorizon/adminrecord.

French-McCay, D.P., Morandi, Alicia, McManus, M.C., Gearon, M. Schroeder, Jayko, K., Rowe, J.J., 2015b. Technical Reports for Deepwater Horizon Water Column Injury Assessment – WC_TR.09: Vertical Distribution Analysis of Plankton. DWH NRDA Water Column Technical Working Group Report. Prepared for National Oceanic and Atmospheric Administration by RPS ASA, South Kingstown, RI, USA. DWH NRDA Water Column Technical Working Group Report. Prepared for National Oceanic and Atmospheric Administration by RPS ASA, South Kingstown, RI, USA. Administrative Record no. DWH-AR0195958.pdf, DWH-AR0171921.xlsx, DWH-AR0171922.xlsx. https://www.doi.gov/deepwaterhorizon/adminrecord.

French-McCay, D.P., McManus, M.C., Balouskus, R., Rowe, J.J., Schroeder, M., Morandi, A., Bohaboy, E., Graham, E., 2015c. Technical Reports for Deepwater Horizon Water Column Injury Assessment: WC_TR.10: Evaluation of Baseline Densities for Calculating Direct Injuries of Aquatic Biota During the Deepwater Horizon Oil Spill. DWH NRDA Water Column Technical Working Group Report. Prepared for National Oceanic and Atmospheric Administration by RPS ASA, South Kingstown, RI, USA. Administrative Record no. DWH-AR0285021.pdf, DWH-AR0285141.xlsx, DWH-AR02851412.xlsx. https://www.doi.gov/deepwaterhorizon/adminrecord.

French-McCay, D.P., Balouskus, R., McManus, M.C., Schroeder, M., Rowe, J.J., Bohaboy, E., 2015d. Technical Reports for Deepwater Horizon Water Column Injury Assessment – WC_TR.12: Evaluation of Production Foregone as the Result of Direct Kill of Fish and Invertebrate Individuals. DWH NRDA Water Column Technical Working Group Report. Prepared for National Oceanic and Atmospheric Administration by RPS ASA, South Kingstown, RI, USA. Administrative Record no. DWH-AR0285169.pdf, DWH-AR0285305.xlsx-DWH-AR0285361.xlsx. https://www.doi.gov/deepwaterhorizon/adminrecord.

French-McCay, D.P., Rowe, J., Balouskus, R., Morandi, A., McManus, R.C., 2015e. Technical Reports for Deepwater Horizon Water Column Injury Assessment – WC_TR.28: Injury Quantification for Planktonic Fish and Invertebrates in Estuarine, Shelf and Offshore Waters. DWH NRDA Water Column Technical Working Group Report. Prepared for National Oceanic and Atmospheric Administration by RPS ASA, South Kingstown, RI, USA. Administrative Record no. DWH-AR0172019.pdf, DWH-AR0172219.xlsx- DWH-AR0172227.xlsx. https://www.doi.gov/deepwaterhorizon/adminrecord.

French-McCay, D.P., Li, Z., Horn, M., Crowley, D., Spaulding, M., Mendelsohn, D., Turner, C., 2016. Modeling oil fate and subsurface exposure concentrations from the Deepwater Horizon oil spill. In: Proceedings of the 39th AMOP Technical Seminar on Environmental Contamination and Response, Emergencies Science Division, Environment Canada, Ottawa, ON, Canada, 39, pp. 115–150.

French-McCay, D., Horn, M., Li, Z., Jayko, K., Spaulding, M., Crowley, D., Mendelsohn, D., 2018a. Modeling distribution fate and concentrations of Deepwater Horizon oil in subsurface waters of the Gulf of Mexico. Chapter 31. In: Stout, S., Wang, Z. (Eds.), Oil Spill Environmental Forensics – Case Studies. Elsevier/Academic Press, pp. 683–736. ISBN: 978-O-12-804434-6.

French-McCay, D.K. Jayko, Li, Z., Horn, M., Isaji, T., Spaulding, M., 2018b. Volume II: appendix II - oil transport and fates model technical manual. In: Galagan, C.W., French-McCay, D., Rowe, J., McStay, L. (Eds.), Simulation Modeling of Ocean Circulation and Oil Spills in the Gulf of Mexico. Volume II: Appendixes, pp. 60–277, 425 p. OCS Study BOEM 2018-040. Obligation No.: M11PC00028. https://espis.boem.gov/finalreports/BOEM_2018-040.pdf.

French-McCay, D., Horn, M., Li, Z., Crowley, D., Spaulding, M., Mendelsohn, D., Jayko, K., Kim, Y., Isaji, T., Fontenault, J., Shmookler, R., Rowe, J., 2018c. Simulation Modeling of Ocean Circulation and Oil Spills in the Gulf of Mexico. Volume III: Data Collection, Analysis and Model Validation. US Department of the Interior, Bureau of Ocean Energy Management, Gulf of Mexico OCS Region, New Orleans, LA. OCS Study BOEM 2018-041; 313 p. Obligation No.: M11PC00028. https://espis.boem.gov/finalreports/BOEM_2018-041.pdf.

French-McCay, D., Crowley, D., Rowe, J., Bock, M., Robinson, H., Wenning, R., Walker, A.H., Joeckel, J., Parkerton, T., 2018d. Comparative risk assessment of spill

response options for a deepwater oil well blowout: part I. Oil spill modeling. Mar. Pollut. Bull. 133, 1001–1015. https://doi.org/10.1016/j.marpolbul.2018.05.042.
French-McCay, D., Crowley, D., McStay, L., 2019. Sensitivity of modeled oil fate and exposure from a subsea blowout to oil droplet sizes, depth, dispersant use, and degradation rates. Mar. Pollut. Bull. 146, 779–793. https://doi.org/10.1016/j.marpolbul.2019.07.038.
French-McCay, D.P., Spaulding, M., Crowley, D., Mendelsohn, D., Fontenault, J., Horn, M., 2021a. Validation of oil trajectory and fate modeling of the Deepwater Horizon oil spill. Front. Mar. Sci. 8 https://doi.org/10.3389/fmars.2021.618463.
French-McCay, D.P., Robinson, H.J., Spaulding, M.L., Li, Z., Horn, M., Gloekler, M.D., Kim, Y.H., Crowley, D., Mendelsohn, D., 2021b. Validation of oil fate and mass balance for the Deepwater Horizon oil spill: evaluation of water column partitioning. Mar. Pollut. Bull. in review.
Fu, J., Gong, Y., Zhao, X., O'Reilly, S.E., Zhao, D., 2014. Effects of oil and dispersant on formation of marine oil snow and transport of oil hydrocarbons. Environ. Sci. Technol. 48 (24), 14392–14399. https://doi.org/10.1021/es5042157.
Garcia-Pineda, O., Zimmer, B., Howard, M., Pichel, W., Li, X., MacDonald, I.R., 2009. Using SAR images to delineate ocean oil slicks with a texture classifying neural network algorithm (TCNNA). Can. J. Remote. Sens. 35 (5), 411–421. https://doi.org/10.5589/m09-035.
Garcia-Pineda, O., MacDonald, I., Hu, C., Svejkovsky, J., Hess, M., Dukhovskoy, D., Morey, S.L., 2013a. Detection of floating oil anomalies from the Deepwater Horizon oil spill with synthetic aperture radar. Oceanography 26 (2), 124–137. https://doi.org/10.5670/oceanog.2013.38.
Garcia-Pineda, O., MacDonald, I.R., Li, X., Jackson, C.R., Pichel, W.G., 2013b. Oil spill mapping and measurement in the Gulf of Mexico with Textural Classifier Neural Network Algorithm (TCNNA). IEEE J. Sel. Top. Appl. Earth Observ. Remote Sens. 6 (6), 2517–2525. https://doi.org/10.1109/JSTARS.2013.2244061.
Goni, G.J., Trinanes, J.A., MacFadyen, A., Streett, D., Olascoaga, M.J., Imhoff, M.L., Muller-Karger, F., Roffer, M.A., 2015. Variability of the Deepwater Horizon surface oil spill extent and its relationship to varying ocean currents and extreme weather conditions. In: Ehrhardt, M. (Ed.), Mathematical Modelling and Numerical Simulation of Oil Pollution Problems. Springer International Publishing Switzerland, pp. 1–22. https://doi.org/10.1007/978-3-319-16459-5_1.
de Gouw, J.A., Middlebrook, A.M., Warneke, C., Ahmadov, R., Atlas, E.L., Bahreini, R., Blake, D.R., Brock, C.A., Brioude, J., Fahey, D.W., Fehsenfeld, F.C., Holloway, J.S., Le Henaff, M., Lueb, R.A., McKeen, S.A., Meagher, J.F., Murphy, D.M., Paris, C., Parrish, D.D., Perring, A.E., Pollack, I.B., Ravishankara, A.R., Robinson, A.L., Ryerson, T.B., Schwarz, J.P., Spackman, J.R., Srinivasan, A., Watts, L.A., 2011. Organic aerosol formation downwind from the Deepwater Horizon oil spill. Science 331, 1295–1299. https://doi.org/10.1126/science.1200320.
Graettinger, G., Holmes, J., Garcia-Pineda, O., Hess, M., Hu, C., Leifer, I., MacDonald, I., Muller-Karger, F., Svejkovsky, J., 2015. Integrating Data from Multiple Satellite Sensors to Estimate Daily Oiling in the Northern Gulf of Mexico during the Deepwater Horizon Oil Spill. DWH Natural Resource Exposure NRDA Technical Working Group Report, FE_TR.31, NOAA, August 31, 2015, 46p. DWH-AR0062925. PDF. https://www.doi.gov/deepwaterhorizon/adminrecord.
Gros, J., Reddy, C.M., Nelson, R.K., Socolofsky, S.A., Arey, J.S., 2016. Simulating gas–liquid–water partitioning and fluid properties of petroleum under pressure: implications for deep-sea blowouts. Environ. Sci. Technol. 50 (14), 7397–7408. https://doi.org/10.1021/acs.est.5b04617.
Gros, J., Socolofsky, S.A., Dissanayake, A.L., Jun, I., Zhao, L., Boufadel, M.C., Reddy, C. M., Arey, J.S., 2017. Petroleum dynamics in the sea and influence of subsea dispersant injection during Deepwater Horizon. Proc. Natl. Acad. Sci. 114 (38), 10065–10070. https://doi.org/10.1073/pnas.1612518114.
Gros, J., Arey, S., Socolofsky, S.A., Dissanayake, A.L., 2020. Dynamics of live oil droplets and natural gas bubbles in deep water. Environ. Sci. Technol. 54 (19), 11865–11875. https://doi.org/10.1021/acs.est.9b06242, 2020.
Hazen, T.C., Dubinsky, E.A., DeSantis, T.Z., Andersen, G.L., Piceno, Y.M., Singh, N., Jansson, J.K., Probst, A., Borglin, S.E., Fortney, J.L., Stringfellow, W.T., Bill, M., Conrad, M.E., Tom, L.M., Chavarria, K.L., Alusi, T.R., Lamendella, R., Joyner, D.C., Spier, C., Baelum, J., Auer, M., Zemla, M.L., Chakraborty, R., Sonnenthal, E.L., 2010. Deep-sea oil plume enriches indigenous oil-degrading bacteria. Science 330 (6001), 204–208. https://doi.org/10.1126/science.1195979.
Hole, L.R., Dagestad, K.-F., Röhrs, J., Wettre, C., Kourafalou, V.H., Androulidakis, Y., Kang, H., Le Hénaff, M., Garcia-Pineda, O., 2019. The DeepWater Horizon oil slick: simulations of river front effects and oil droplet size distribution. J. Mar. Sci. Eng. 7 (10), 329. https://doi.org/10.3390/jmse7100329.
Horn, M., French-McCay, D., Payne, J., Driskell, W., Li, Z., Grennan, M., Decker, L., Zamorski, S., 2015. Technical Reports for Deepwater Horizon Water Column Injury Assessment –Volume III. Water Column Chemical and Physical Data from the Deep Water Horizon Blowout. RPS ASA, South Kingstown, RI, USA, August 2015. DWH-AR0024617.pdf (main), DWH-AR0024364.pdf (Appendix B), DWH-AR0024462.pdf (Appendix C), DWH-AR0023990.pdf (Appendix D). https://www.doi.gov/deepwaterhorizon/adminrecord.
Hu, C., Li, X., Pichel, W.G., Muller-Karger, F.E., 2009. Detection of natural oil slicks in the NW Gulf of Mexico using MODIS imagery. Geophys. Res. Lett. 36 https://doi.org/10.1029/2008gl036119.
Hu, C., Weisberg, R.H., Liu, Y., Zheng, L., Daly, K.L., English, D.C., Zhao, J., Vargo, G.A., 2011. Did the northeastern Gulf of Mexico become greener after the Deepwater Horizon oil spill? Geophys. Res. Lett. 38 (9), L09601. https://doi.org/10.1029/2011GL047184.
Johansen, Ø., 2000. DeepBlow – a Lagrangian plume model for deep water blowouts. Spill Sci. Technol. Bull. 6, 103–111. https://doi.org/10.1016/S1353-2561(00)00042-6.
Johansen, Ø., 2003. Development and verification of deep-water blowout models. Mar. Pollut. Bull. 47, 360–368. https://doi.org/10.1016/S0025-326X(03)00202-9.
Johansen, O., Brandvik, P., Farook, U., 2013. Droplet breakup in subsea oil releases – part 2: predictions of droplet size distributions with and without injection of chemical dispersants. Mar. Pollut. Bull. 73, 327–335. https://doi.org/10.1016/j.marpolbul.2013.04.012.
Jolliff, J.K., Smith, T.A., Ladner, S., Arnone, R.A., 2014. Simulating surface oil transport during the Deepwater Horizon oil spill: experiments with the BioCast system. Ocean Modell. 75, 84–99. https://doi.org/10.1016/j.ocemode.2014.01.004.
Joye, S.B., 2015. Deepwater Horizon, 5 years on. Science 349, 592–593. https://doi.org/10.1126/science.aab4133.
Joye, S., MacDonald, I.R., Leifer, I., Asper, V., 2011. Magnitude and oxidation potential of hydrocarbon gases released from the BP oil well blowout. Nat. Geosci. 4, 160–164. https://doi.org/10.1038/ngeo1067.
Joye, S.B., Teske, A.P., Kostka, J.E., 2014. Microbial dynamics following the Macondo oil well blowout across Gulf of Mexico environments. BioScience 64, 766–777. https://doi.org/10.1093/biosci/biu121.
Joye, S.B., Bracco, A., Özgökmen, T.M., Chanton, J.P., Grosell, M., MacDonald, I.R., Cordes, E.E., Montoya, J.P., Passow, U., 2016. The Gulf of Mexico ecosystem, six years after the Macondo oil well blowout. Deep-Sea Res. II Top. Stud. Oceanogr. 129, 4–19. https://doi.org/10.1016/j.dsr2.2016.04.018.
Kessler, J.D., Valentine, D.L., Redmond, M.C., Du, M., Chan, E.W., Mendes, S.D., Quiroz, E.W., Villanueva, C.J., Shusta, S.S., Werra, L.M., Yvon-Lewis, S.A., Weber, T. C., 2011. A persistent oxygen anomaly reveals the fate of spilled methane in the deep Gulf of Mexico. Science 331, 312–315. https://doi.org/10.1126/science.1199697.
Kirstein, B.E., Clayton, J.R., Clary, C., Payne, J.R., McNabb Jr., D., Fauna, G., Redding, R., 1987. Integration of Suspended Particulate Matter and Oil Transportation Study. Minerals Management Service, OCS Study MMS87-0083, Anchorage, Alaska, 216p. https://marinecadastre.gov/espis/#/search/study/25918.
Kourafalou, V.H., Androulidakis, Y.S., 2013. Influence of Mississippi River induced circulation on the Deepwater Horizon oil spill transport. J. Geophys. Res. 118 (8), 3,823–3,842. https://doi.org/10.1002/jgrc.20272.
Kujawinski, E.B., Kido Soule, M.C., Valentine, D.L., Boysen, A.K., Longnecker, K., Redmond, M.C., 2011. Fate of dispersants associated with the Deepwater Horizon oil spill. Environ. Sci. Technol. 45, 1298–1306. https://doi.org/10.1021/es103838p.
Le Hénaff, M., Kourafalou, V.H., Paris, C.B., Helgers, J., Aman, Z.M., Hogan, P.J., Srinivasan, A., 2012. Surface evolution of the Deepwater Horizon oil spill patch: combined effects of circulation and wind-induced drift. Environ. Sci. Technol. 46 (13), 7267–7273. https://doi.org/10.1021/es301570w.
Lehr, W., Bristol, S., Possolo, A., et al., 2010. Oil Budget Calculator, Deepwater Horizon, Technical Documentation. A Report to the National Incident Command. The Federal Interagency Solutions Group, Oil Budget Calculator Science and Engineering Team. http://www.restorethegulf.gov/sites/default/files/documents/pdf/OilBudgetCalc_Full_HQ-Print_111110.pdf. November 2010. (Accessed on April 1, 2012).
Leifer, I., Lehr, W.J., Simecek-Beatty, D., Bradley, E., Clark, R., Dennison, P., Hu, Y., Matheson, S., Jones, C.E., Holt, B., Reif, M., Roberts, D.A., Svejkovsky, J., Swayze, G., Wozencraft, J., 2012. State of the art satellite and airborne marine oil spill remote sensing: application to the BP Deepwater Horizon oil spill. Remote Sens. Environ. 124, 185–209. https://doi.org/10.1016/j.rse.2012.03.024.
Li, Z., Bird, A., Payne, J.R., Vinhateiro, N., Kim, Y., Davis, C., Loomis, N., 2015. Technical Reports for Deepwater Horizon Water Column Injury Assessment – Volume IV. Oil Particle Data from the Deepwater Horizon Oil Spill. RPS ASA, South Kingstown, RI, USA, August 2015. DWH-AR0024715.pdf. https://www.doi.gov/deepwaterhorizon/adminrecord.
Li, Z., Spaulding, M.L., French-McCay, D., Crowley, D., Payne, J.R., 2017a. Development of a unified oil droplet size distribution model with application to surface breaking waves and subsea blowout releases considering dispersant effects. Mar. Pollut. Bull. 114 (1), 247–257. https://doi.org/10.1016/j.marpolbul.2016.09.008.
Li, Z., Spaulding, M., French-McCay, D., 2017b. An algorithm for modeling entrainment and naturally and chemically dispersed oil droplet size distribution under surface breaking wave conditions. Mar. Pollut. Bull. 119 (1), 145–152. https://doi.org/10.1016/j.marpolbul.2017.03.048.
Lindo-Atichati, D., Paris, C.B., Le Hénaff, M., Schedler, M., Juárez, A.G. Valladares, Müller, R., 2016. Simulating the effects of droplet size, high-pressure biodegradation, and variable flow rate on the subsea evolution of deep plumes from the Macondo blowout. Deep Sea Res. Part II: Top. Stud. Oceanogr. (0) https://doi.org/10.1016/j.dsr2.2014.01.011.
Liu, Y., Weisberg, R.H., Hu, C., Zheng, L., 2011. Tracking the Deepwater Horizon oil spill: a modeling perspective. EOS Trans. Am. Geophys. Union 92 (6), 45–46. https://doi.org/10.1029/2011EO060 0 01.
Mabile, N., Allen, A., 2010. Controlled Burns After Action Report, Burns on May 28th–August 3, 2010. Controlled Burn Group, Report prepared by Nere' Mabile & Al Allen. August 8, 2010, 28p. https://www.erma.noaa.gov/gulfofmexico/erma.html. https://prod-erma-api.orr.noaa.gov/api/v1/data_layer_file/2436/download/.
MacDonald, I.R., Garcia-Pineda, O., Beet, A., Daneshgar Asl, S., Feng, L., Graettinger, G., French-McCay, D., Holmes, J., Hu, C., Huffer, F., Leifer, I., Muller-Karger, F., Solow, A., Silva, M., Swayze, G., 2015. Natural and unnatural oil slicks in the Gulf of Mexico. J. Geophys. Res. Oceans 120 (8), 364–368. https://doi.org/10.1002/2015JC011062.
MacFadyen, A., Watabayashi, G.Y., Barker, C.H., Beegle-Krause, C.J., 2011. Tactical modeling of surface oil transport during the Deepwater Horizon spill response. In: Liu, Y., MacFadyen, A., Ji, Z.-G., Weisberg, R.H. (Eds.), Monitoring and Modeling the Deepwater Horizon Oil Spill: A Record-Breaking Enterprise. American Geophysical Union, Washington, DC, pp. 167–178. https://doi.org/10.1029/2011GM001128.

Mariano, A., Kourafalou, V., Srinivasan, A., Kang, H., Halliwell, G., Ryan, E., Roffer, M., 2011. On the modeling of the 2010 Gulf of Mexico oil spill. Dyn. Atmos. Oceans 52 (1), 322–340. https://doi.org/10.1016/j.dynatmoce.2011.06.001.

McNutt, M.K., Camilli, R., Crone, T.J., Guthrie, G.D., Hsieh, P.A., Ryerson, T.B., Savas, O., Shaffer, F., 2012a. Review of flow rate estimates of the Deepwater Horizon oil spill. Science applications in the Deepwater Horizon oil spill special feature. Proc. Natl. Acad. Sci. 109 (50), 20260–20267. https://doi.org/10.1073/pnas.1112139108.

McNutt, M.K., Chu, S., Lubchenco, J., Hunter, T., Dreyfus, G., Murawski, S.A., Kennedy, D.M., 2012b. Applications of science and engineering to quantify and control the Deepwater Horizon oil spill. Proc. Natl. Acad. Sci. U. S. A. 109, 20222–20228. https://doi.org/10.1073/pnas.1214389109.

Montagna, P.A., Baguley, J.G., Cooksey, C., Hartwell, I., Hyde, L.J., Hyland, J.L., Kalke, R.D., Kracker, L.M., Reuscher, M., Rhodes, A.C.E., 2013. Deep-sea benthic footprint of the Deepwater Horizon blowout. PLoS One 8 (8), e70540. https://doi.org/10.1371/journal.pone.0070540.

National Academies of Sciences, Engineering, and Medicine (NASEM), 2020. The Use of Dispersants in Marine Oil Spill Response. The National Academies Press, Washington, DC. https://doi.org/10.17226/25161, 340p.

Nissanka, I.D., Yapa, P.D., 2016. Calculation of oil droplet size distribution in an underwater oil well blowout. J. Hydraul. Res. 54 (3), 307–320. https://doi.org/10.1080/00221686.2016.1144656.

Nixon, Z., Zengel, S., Baker, M., Steinhoff, M., Fricano, G., Rouhani, S., Michel, J., 2016. Shoreline oiling from the Deepwater Horizon oil spill. Mar. Pollut. Bull. 107, 170–178. https://doi.org/10.1016/j.marpolbul.2016.04.003.

North, E.W., Adams, E.E., Schlag, Z., Sherwood, C.R., He, R., Hyun, K.H., Socolofsky, S. A., 2011. Simulating oil droplet dispersal from the Deepwater Horizon spill with a Lagrangian approach. In: Liu, Y., MacFadyen, A., Ji, Z.-G., Weisberg, R.H. (Eds.), Monitoring and Modeling the Deepwater Horizon Oil Spill: A Record-Breaking Enterprise. American Geophysical Union, Washington, D.C., pp. 217–226

North, E.W., Adams, E.E., Thessen, A.E., Schlag, Z., He, R., Socolofsky, S.A., Masutani, S. M., Peckham, S.D., 2015. The influence of droplet size and biodegradation on the transport of subsurface oil droplets during the Deepwater Horizon spill: a model sensitivity study. Environ. Res. Lett. 10 (2), 024016. https://doi.org/10.1088/1748-9326/10/2/024016.

Operational Science Advisory Team (OSAT), 2011. Summary Report for Sub-Sea and Sub-Surface Oil and Dispersant Detection: Ecotoxicity Addendum. Report prepared by the Operational Science Advisory Team (OSAT), Gulf Coast Incident Management Team, for the US Coast Guard, 8 July 2011. https://restorethegulf.gov/release/2015/07/01/osat-summary-report-sub-sea-and-sub-surface-oil-and-dispersant-detection.

Operational Science Advisory Team 2 (OSAT-2), 2011. Summary Report for Fate and Effects of Remnant Oil in the Beach Environment. Operational Science Advisory Team (OSAT-2), Gulf Coast Incident Management Team. Prepared for Lincoln D. Stroh, CAPT, U.S. Coast Guard, Federal On-Scene Coordinator, Deepwater Horizon MC252. February 10, 2011. https://restorethegulf.gov/release/2015/07/01/osat-2-fate-and-effects-oil-beaches.

Özgökmen, T.M., Chassignet, E.P., Dawson, C.N., Dukhovskoy, D., Jacobs, G., Ledwell, J., Garcia-Pineda, O., MacDonald, I.R., Morey, S.L., Olascoaga, M.J., Poje, A.C., Reed, M., Skancke, J., 2016. Over what area did the oil and gas spread during the 2010 Deepwater Horizon oil spill? Oceanography 29 (3), 96–107. https://doi.org/10.5670/oceanog.2016.74.

Paquin, P.R., McGrath, J., Fanelli, C.J., Di Toro, D.M., 2018. The aquatic hazard of hydrocarbon liquids and gases and the modulating role of pressure on dissolved gas and oil toxicity. Mar. Pollut. Bull. 133, 930–942. https://doi.org/10.1016/j.marpolbul.2018.04.051.

Paris, C.B., Hénaff, M.L., Aman, Z.M., Subramaniam, A., Helgers, J., Wang, D.-P., Kourafalou, V.H., Srinivasan, A., 2012. Evolution of the Macondo well blowout: simulating the effects of the circulation and synthetic dispersants on the subsea oil transport. Environ. Sci. Technol. 46, 13293–13302. https://doi.org/10.1021/es303197h.

Passow, U., 2016. Formation of rapidly-sinking, oil-associated marine snow. Deep Res. Part II Top. Stud. Oceanogr. 129, 232–240. https://doi.org/10.1016/j.dsr2.2014.10.001.

Passow, U., Hetland, R.D., 2016. What happened to all of the oil? Oceanography 29 (3), 88–95. https://doi.org/10.5670/oceanog.2016.73.

Passow, U., Overton, E.B., 2021. The complexity of spills: the fate of the Deepwater Horizon oil. Annu. Rev. Mar. Sci. 13, 109–136. https://doi.org/10.1146/annurev-marine-032320-095153.

Passow, U., Stout, S.A., 2020. Character and sedimentation of "lingering" Macondo oil to the deep-sea after the Deepwater Horizon oil spill. Mar. Chem. 218, 103733 https://doi.org/10.1016/j.marchem.2019.103733.

Passow, U., Ziervogel, K., 2016. Marine snow sedimented oil released during the Deepwater Horizon spill. Oceanography 29 (3), 118–125. https://doi.org/10.5670/oceanog.2016.76.

Passow, U., Ziervogel, K., Asper, V., Diercks, A., 2012. Marine snow formation in the aftermath of the Deepwater Horizon oil spill in the Gulf of Mexico. Environ. Res. Lett. 7 https://doi.org/10.1088/1748-9326/7/3/035301.

Payne, J.R., Driskell, W.B., 2015a. 2010 DWH offshore water column samples—forensic assessments and oil exposures. PECI technical report to the trustees in support of the PDARP. In: U.S. Dept. of Interior, Deepwater Horizon Response & Restoration, Admin. Record. www.doi.gov/deepwaterhorizon/adminrecord (DWH-AR0039118, 37 pp.).

Payne, J.R., Driskell, W.B., 2015b. Deepwater Horizon oil spill NRDA offshore adaptive sampling strategies and field observations. PECI technical report to the trustees in support of the PDARP. In: U.S. Dept. of Interior, Deepwater Horizon Response & Restoration, Admin. Record. www.doi.gov/deepwaterhorizon/adminrecord (DWHAR0023786, 75 pp.).

Payne, J.R., Driskell, W.B., 2015c. Forensic fingerprinting methods and classification of DWH offshore water samples. PECI technical report to the trustees in support of the PDARP. In: U.S. Dept. of Interior, Deepwater Horizon Response & Restoration, Admin. Record. www.doi.gov/deepwaterhorizon/adminrecord (DWH-AR0039170, 31 pp.).

Payne, J.R., Driskell, W.B., 2015d. Dispersant effects on waterborne oil profiles and behavior during the Deepwater Horizon oil spill. PECI technical report to the trustees in support of the PDARP. In: U.S. Dept. of Interior, Deepwater Horizon Response & Restoration, Admin. Record. www.doi.gov/deepwaterhorizon/adminrecord (DWH-AR0039201, 22 p. DWH NRDA Chemistry Technical Working Group Report, August 30, 2015).

Payne, J.R., Driskell, W.B., 2016. Water column sampling for forensics. In: Stout, S., Wang, Z. (Eds.), Standard Handbook Oil Spill Environmental Forensics – Fingerprinting and Source Identification, 2nd edition. Elsevier/Academic Press, pp. 983–1014.

Payne, J.R., Driskell, W.B., 2017. Water-column measurements and observations from the Deepwater Horizon oil spill natural resource damage assessment. Int. Oil Spill Conf. Proc. 2017 (1), 3071–3090. https://doi.org/10.7901/2169-3358-2017.1.3071.

Payne, J.R., Driskell, W.B., 2018. Macondo oil in northern Gulf of Mexico waters – part 1: assessments and forensic methods for Deepwater Horizon offshore water samples. Mar. Pollut. Bull. 129, 399–411. https://doi.org/10.1016/j.marpolbul.2018.02.055.

Payne, J.R., Flynn, N.W., Mankiewicz, P.J., Smith, G.S., 1980. Subsurface evaporation/dissolution partitioning of lower-molecular-weight aromatic hydrocarbons in a down-plume transect from the IXTOC I wellhead. In: Proceedings of the Symposium on Preliminary Results from the September 1979 Researcher/Pierce IXTOC I Cruise. Key Biscayne, Florida, June 9–10, 1980, Volume 55, U.S. Dept. of Commerce, National Oceanic and Atmospheric Administration, Office of Marine Pollution Assessment, Boulder Colorado, pp. 239–263, 591p. (NTIS Accession Number PB-246068. ISBN-13: 9781001206858).

Payne, J.R., Kirstein, B.E., McNabb Jr., G.D., Lambach, J.L., Redding, R., Jordan, R.E., Hom, W., de Oliveria, C., Smith, G.S., Baxter, D.M., Gaegel, R., 1984. Multivariate analysis of petroleum weathering in the marine environment – sub Arctic. In: Environmental Assessment of the Alaskan Continental Shelf, OCEAP, Final Report of Principal Investigators, vol. 21 and 22. U.S. Department of Commerce, National Oceanic and Atmospheric Administration, Ocean Assessment Division, Juneau, Alaska. Feb. 1984, 690p. https://marinecadastre.gov/espis/#/search/study/25918.

Payne, J.R., Kirstein, B.E., Clayton Jr., J.R., Clary, C., Redding, R., McNabb Jr., G.D., Farmer, G., 1987. Integration of suspended particulate matter and oil transportation study. In: Final Report. Minerals Management Service, Environmental Studies Branch, Anchorage, AK. Contract No. 14-12-0001-30146, 216 p. https://www.boem.gov/sites/default/files/boem-newsroom/Library/Publications/1987/87_0083.pdf.

Perlin, N., Paris, C.B., Berenshtein, I., Vaz, A.C., Faillettaz, R., Aman, Z.M., Schwing, P.T., Romero, I.C., Schlüter, M., Liese, A., 2020. Far-field modeling of a deep-sea blowout: sensitivity studies of initial conditions, biodegradation, sedimentation, and subsurface dispersant injection on surface slicks and oil plume concentrations. In: Deep Oil Spills. Springer, pp. 170–192.

Quigg, A., Passow, U., Chin, W.-C., Bretherton, L., Kamalanathan, M., Xu, C., Schwehr, K. A., Zhang, S., Sun, L., Wade, T.L., Finkel, Z.V., Doyle, S., Sylvan, J.B., Williams, A.K., Obeid, W., Hatcher, P.G., Knap, A.H., Santschi, P.H., 2016. The role of microbial exopolymers in determining the fate of oil and chemical dispersants in the ocean. Limnol. Oceanogr. Lett. 1, 3–26. https://doi.org/10.1002/lol2.10030.

Reddy, C.M., Arey, J.S., Seewald, J.S., Sylva, S.P., Lemkau, K.L., Nelson, R.K., Van Mooy, M.A.S., Camilli, R., 2012. Composition and fate of gas and oil released to the water column during the Deepwater Horizon oil spill. Proc. Natl. Acad. Sci. 109 (5), 20229–20234. https://doi.org/10.1073/pnas.1101242108.

Romero, I.C., Schwing, P.T., Brooks, G.R., Larson, R.A., Hastings, D.W., Flower, B.P., Goddard, E.A., Hollander, D.J., 2015. Hydrocarbons in deep-sea sediments following the 2010 Deepwater Horizon blowout in the Northeast Gulf of Mexico 1-23. PLoS One 10 (5), e0128371. https://doi.org/10.1371/journal.pone.0128371.

Romero, I.C., Toro-Farmer, G., Diercks, A.-R., Schwing, P., Muller-Karger, F., Murawski, S., Hollander, D.J., 2017. Large-scale deposition of weathered oil in the Gulf of Mexico following a deep-water oil spill. Environ. Pollut. 228, 179–189. https://doi.org/10.1016/j.envpol.2017.05.019.

Rye, H., 1994. Model for calculation of underwater blow-out plume. In: Proceedings of 17th Arctic Marine Oil Spill Program (AMOP) Technical Seminar. Emergencies Science Division, Environment Canada, Ottawa, ON, Canada, pp. 849–865, 17(2).

Rye, H., Brandvik, P.J., 1997. Verification of subsurface oil spill models. Int. Oil Spill Conf. Proc. 1997 (1), 551–557. https://doi.org/10.7901/2169-3358-1997-1-551.

Ryerson, T.B., Aikin, K.C., Angevine, W.M., Atlas, E.L., Blake, D.R., Brock, C.A., Fehsenfeld, F.C., Gao, R.-S., de Gouw, J.A., Fahey, D.W., Holloway, J.S., Lack, D.A., Lueb, R.A., Meinardi, S., Middlebrook, A.M., Murphy, D.M., Neuman, J.A., Nowak, J. B., Parrish, D.D., Peischl, J., Perring, A.E., Pollack, I.B., Ravishankara, A.R., Roberts, J.M., Schwarz, J.P., Spackman, J.R., Stark, H., Warneke, C., Watts, L.A., 2011. Atmospheric emissions from the Deepwater Horizon spill constrain air-water partitioning, hydrocarbon fate, and leak rate. Geophys. Res. Lett. 38, L07803. https://doi.org/10.1029/2011GL046726.

Ryerson, T.B., Camilli, R., Kessler, J.D., Kujawinski, E.B., Reddy, C.M., Valentine, D.L., Atlas, E., Blake, D.R., De Gouw, J., Meinardi, S., Parrish, D.D., Peischl, J., Seewald, J. S., Warneke, C., 2012. Chemical data quantify Deepwater Horizon hydrocarbon flow rate and environmental distribution. Proc. Natl. Acad. Sci. 109 (50), 20246–20253. https://doi.org/10.1073/pnas.1110564109.

Salisbury, J.E., Campbell, J.W., Linder, E., Meeker, L.D., Muller-Karger, F.E., Vorosmarty, C.J., 2004. On the seasonal correlation of surface particle fields with

wind stress and Mississippi discharge in the northern Gulf of Mexico. Deep-Sea Res. II 51, 1187–1203. https://doi.org/10.1016/j.dsr2.2004.03.002.
Socolofsky, S.A., Adams, E.E., 2002. Multi-phase plumes in uniform and stratified crossflow. J. Hydraul. Res. 40, 661–672. https://doi.org/10.1080/00221680209499913.
Socolofsky, S.A., Adams, E.E., Sherwood, C.R., 2011. Formation dynamics of subsurface hydrocarbon intrusions following the Deepwater Horizon blowout. Geophys. Res. Lett. 38 (9), L09602. https://doi.org/10.1029/2011GL047174.
Socolofsky, S.A., Dissanayake, A.L., Jun, I., Gros, J., Arey, J.S., Reddy, C.M., 2015a. Texas A&M Oilspill Calculator (TAMOC) modeling suite for subsea spills. In: Proceedings of the 38th AMOP Technical Seminar, 38. Emergencies Science Division, Environment Canada, Ottawa, ON, Canada, pp. 153–168.
Socolofsky, S.A., Adams, E.E., Boufadel, M.C., Aman, Z.M., Johansen, Ø., Konkel, W.J., Lindo, D., Madsen, M.N., North, E.W., Paris, C.B., Rasmussen, D., Reed, M., Rønningen, P., Sim, L.H., Uhrenholdt, T., Anderson, K.G., Cooper, C., Nedwed, T.J., 2015b. Intercomparison of oil spill prediction models for accidental blowout scenarios with and without subsea chemical dispersant injection. Mar. Pollut. Bull. 96 (1–2), 110–126. https://doi.org/10.1016/j.marpolbul.2015.05.039.
Spaulding, M.L., Bishnoi, P.R., Anderson, E., Isaji, T., 2000. An integrated model for prediction of oil transport from a deep water blowout. In: Proceedings of the 23rd AMOP Technical Seminar on Environmental Contamination and Response, 23. Emergencies Science Division, Environment Canada, Ottawa, ON, Canada, pp. 611–636.
Spaulding, M.L., Mendelsohn, D., Crowley, D., Li, Z., Bird, A., 2015. Draft Technical Reports for Deepwater Horizon Water Column Injury Assessment: WC_TR.13: Application of OILMAP DEEP to the Deepwater Horizon Blowout. DWH NRDA Water Column Technical Working Group Report. Prepared for National Oceanic and Atmospheric Administration by RPS ASA, South Kingstown, RI 02879. Administrative Record no. DWH-AR0285366.pdf. https://www.doi.gov/deepwaterhorizon/adminrecord.
Spaulding, M., Li, Z., Mendelsohn, D., Crowley, D., French-McCay, D., Bird, A., 2017. Application of an integrated blowout model system, OILMAP DEEP, to the Deepwater Horizon (DWH) spill. Mar. Pollut. Bull. 120, 37–50. https://doi.org/10.1016/j.marpolbul.2017.04.043.
Spier, C., Stringfellow, W.T., Hazen, T.C., Conrad, M., 2013. Distribution of hydrocarbons released during the 2010 MC252 oil spill in deep offshore waters. Environ. Pollut. 173 (0), 224–230. https://doi.org/10.1016/j. envpol.2012.10.019 (PMID: 23202654).
Stout, S.A., 2015a. Physical and chemical properties of the fresh MC252 Macondo-1 well crude oil. NewFields Technical Report to the Trustees in support of the pDARP. In: U. S. Dept. of Interior, Deepwater Horizon Response & Restoration, Admin. Record, p. 21. www.doi.gov/deepwaterhorizon/adminrecord. Report DWH-AR0038495.
Stout, S.A., 2015b. Bulk chemical and physical properties of fresh and weathered Macondo crude oil. NewFields Technical Report to the Trustees in support of the pDARP. U.S. Dept. of Interior, Deepwater Horizon Response & Restoration, Admin. Record 18. Report DWH-AR0038585, 11p and Attachment DWH-AR0038567. www.doi.gov/deepwaterhorizon/adminrecord.
Stout, S.A., German, C.R., 2018. Characterization and flux of marine oil snow settling toward the seafloor in the northern Gulf of Mexico during the Deepwater Horizon incident: evidence for input from surface oil and impact on shallow shelf sediments. Mar. Pollut. Bull. 129 (2), 695–713. https://doi.org/10.1016/j.marpolbul.2017.10.059.
Stout, S.A., Payne, J.R., 2016a. Macondo oil in deep-sea sediments: part 1 – sub-sea weathering of oil deposited on the seafloor. Mar. Pollut. Bull. 111, 365–380. https://doi.org/10.1016/j.marpolbul.2016.07.041.
Stout, S.A., Payne, J.R., 2016b. Chemical composition of floating and sunken in-situ burn residues from the Deepwater Horizon oil spill. Mar. Pollut. Bull. 108, 186–202. https://doi.org/10.1016/j.marpolbul.2016.04.031.
Stout, S.A., Payne, J.R., 2017. Footprint, weathering, and persistence of synthetic-base drilling mud olefins in deep-sea sediments following the Deepwater Horizon disaster. Mar. Pollut. Bull. 118 (1–2), 328–340. https://doi.org/10.1016/j.marpolbul.2017.03.013.
Stout, S.A., Payne, J.R., Emsbo-Mattingly, S.D., Baker, G., 2016a. Weathering of field-collected floating and stranded Macondo oils during and shortly after the Deepwater Horizon oil spill. Mar. Pollut. Bull. 105 (1), 7–22. https://doi.org/10.1016/j.marpolbul.2016.02.044.
Stout, S.A., Payne, J.R., Ricker, R.W., Baker, G., Lewis, C., 2016b. Macondo oil in deep-sea sediments: part 2 – distribution and distinction from background and natural oil seeps. Mar. Pollut. Bull. 111, 381–401. https://doi.org/10.1016/j.marpolbul.2016.07.041.
Stout, S.A., Rouhani, S., Liu, B., Oehrig, J., Ricker, R.W., Baker, G., Lewis, C., 2017. Assessing the footprint and volume of oil deposited in deep-sea sediments following the Deepwater Horizon oil spill. Mar. Pollut. Bull. 114, 327–342. https://doi.org/10.1016/j.marpolbul.2016.09.046.
Svejkovsky, J., Hess, M., 2012. Expanding the utility of remote sensing data for oil spill response. Photogramm. Eng. Remote Sens. 78 (10), 1011–1014.
Svejkovsky, J., Lehr, W., Muskat, J., Graettinger, G., Mullin, J., 2012. Operational utilization of aerial multispectral remote sensing during oil spill response: lessons learned during the Deepwater Horizon (MC-252) spill. Photogramm. Eng. Remote. Sens. 78 (10), 1089–1102. https://doi.org/10.14358/PERS.78.10.1089.
Svejkovsky, J., Hess, M., Muskat, J., Nedwed, T.J., McCall, J., Garcia, O., 2016. Characterization of surface oil thickness distribution patterns observed during the Deepwater Horizon (MC-252) oil spill with aerial and satellite remote sensing. Mar. Pollut. Bull. 110 (1), 162–176. https://doi.org/10.1016/j.marpolbul.2016.06.066.
Testa, J.M., Adams, E.E., North, E.W., He, R., 2016. Modeling the influence of deep water application of dispersants on the surface expression of oil: a sensitivity study. J. Geophys. Res. Oceans 121, 5995–6008. https://doi.org/10.1002/2015JC011571.
U.S. District Court (USDC), 2015. Findings of Facts and Conclusions of Law - Phase 2 Trial. Case 2: 10-md-02179-cjb-ss, p. 1e44. Document 14021 Filed Jan. 15, 2015. http://www.laed.uscourts.gov/sites/default/files/OilSpill/Orders/1152015FindingsPhaseTwo.pdf.
Valentine, D.L.K., Kessler, J.D., Redmond, M.C., Mendes, S.D., Heintz, M.B., Farwell, C., Hu, L., Kinnaman, F.S., Yvon-Lewis, S., Du, M., Chan, E.W., Tigreros, F.G., Villanueva, C.J., 2010. Propane respiration jump-starts microbial response to a deep oil spill. Science 330, 208–211. https://doi.org/10.1126/science.1196830.
Valentine, D.L., Fisher, G.B., Bagby, S.C., Nelson, R.K., Reddy, C.M., Sylva, S.P., Woo, M. A., 2014. Fallout plume of submerged oil from Deepwater Horizon. Proc. Natl. Acad. Sci. PNAS. 111 (45), 15906–15911. https://doi.org/10.1073/pnas.1414873111.
Ward, C.P., Overton, E.B., 2020. How the 2010 Deepwater Horizon spill reshaped our understanding of crude oil photochemical weathering at sea: a past, present, and future perspective. Environ. Sci. Process. Impacts 22, 1125–1138. https://doi.org/10.1039/d0em00027b.
Ward, C.P., Sharpless, C.M., Valentine, D.L., French-McCay, D.P., Aeppli, C., White, H.K., Rodgers, R.P., Gosselin, K.M., Nelson, R.K., Reddy, C.M., 2018. Partial photochemical oxidation was a dominant fate of Deepwater Horizon surface oil. Environ. Sci. Technol. 52 (4), 1797–1805. https://doi.org/10.1021/acs.est.7b05948.
Weisberg, R.H., Zheng, L., Liu, Y., 2017. On the movement of Deepwater Horizon oil to northern Gulf beaches. Ocean Model. 111, 81–97. https://doi.org/10.1016/j.ocemod.2017.02.002.
Yan, B., Passow, U., Chanton, J.P., Nöthig, E.-M., Apser, V., Sweet, J., Pitiranggon, M., Diercks, A., Pak, D., 2016. Sustained deposition of contaminants from the Deepwater Horizon spill. Proc. Natl. Acad. Sci. 113 (24), E3332–E3340. https://doi.org/10.1073/pnas.1513156113.
Yapa, P.D., Zheng, L., Chen, F.H., 2001. A model for deepwater oil/gas blowouts. Mar. Pollut. Bull. 43, 234–241. https://doi.org/10.1016/S0025-326X(01)00086-8.
Zhao, L., Boufadel, M.C., Socolofsky, S.A., Adams, E., King, T., Lee, K., 2014a. Evolution of droplets in subsea oil and gas blowouts: development and validation of the numerical model VDROP-J. Mar. Pollut. Bull. 83, 58–69. https://doi.org/10.1016/j.marpolbul.2014.04.020.
Zhao, L., Torlapati, J., Boufadel, M.C., King, T., Robinson, B., Lee, K., 2014b. VDROP: a comprehensive model for droplet formation of oils and gases in liquids — incorporation of the interfacial tension and droplet viscosity. Chem. Eng. J. 253, 93–106. https://doi.org/10.1016/j.cej.2014.04.082.
Zhao, L., Boufadel, M.C., Adams, E., Socolofsky, S.A., King, T., Lee, K., Nedwed, T., 2015. Simulation of scenarios of oil droplet formation from the Deepwater Horizon blowout. Mar. Pollut. Bull. 101 (1), 304–319. https://doi.org/10.1016/j.marpolbul.2015.10.068.
Zhao, L., Boufadel, M.C., King, T., Robinson, B., Gao, F., Socolofsky, S.A., Lee, K., 2017a. Droplet and bubble formation of combined oil and gas releases in subsea blowouts. Mar. Pollut. Bull. 120, 203–216. https://doi.org/10.1016/j.marpolbul.2017.05.010.
Zhao, L., Gao, F., Boufadel, M.C., King, T., Robinson, B., Lee, K., Conmy, R., 2017b. Oil jet with dispersant: macro-scale hydrodynamics and tip streaming. AICHE J. 63 (11), 5222–5234. https://doi.org/10.1002/aic.15864.
Zheng, L., Yapa, P.D., Chen, F., 2003. A model for simulating deepwater oil and gas blowouts - part I: theory and model formulation. J. Hydraul. Res. 41 (4), 339–351. https://doi.org/10.1080/00221680309499980.
Ziervogel, K., Joye, S.B., Arnosti, C., 2014. Microbial enzymatic activity and secondary production in sediments affected by the sedimentation pulse following the Deepwater Horizon oil spill. Deep-Sea Res. II. https://doi.org/10.1016/j.dsr2.2014.04.003.